International Journal of Multiphase Flow 35 (2009) 1051–1065

Contents lists available at ScienceDirect

International Journal of Multiphase Flow

journal homepage: www.elsevier.com/locate/ijmulflow

The EHD-driven fluid flow and deformation of a liquid jet by a transverse electric field

Marrivada Nanchara Reddy, Asghar Esmaeeli *

Department of Mechanical Engineering & Energy Processes, Southern Illinois University, Carbondale, IL 62901, USA

ARTICLE INFO

Article history:
Received 5 February 2009
Received in revised form 6 May 2009
Accepted 27 June 2009
Available online 8 July 2009

Keywords:
Electrohydrodynamics
Leaky-dielectric fluids
Liquid jet
Drop deformation
Creeping flow

ABSTRACT

The aim of this study is to investigate the effect of a uniform transverse electric field on the steady-state behavior of a liquid cylinder surrounded by another liquid of infinite extent. The governing electrohydrodynamic equations are solved for Newtonian and immiscible fluids in the framework of leaky-dielectric theory and in the limit of small electric field and fluid inertia. A detailed analysis of the electrical and hydrodynamic stresses acting on the interface separating the two fluids is presented, and an expression is found for the interface deformation for small distortions from a circular shape. The electrical stresses acting on the interface of two leaky-dielectric liquids are compared with those acting on an interface separating a perfect dielectric or infinitely conducting core fluid cylinder from a surrounding perfect dielectric fluid. A comparison is made between the results of this study and those of a similar study for fluids with permeable interfaces and the classical results for liquid drops.

1. Introduction

When a droplet of a fluid is suspended in another fluid and is subjected to an electric field, the mismatch between the dielectric properties of the fluids results in electrical stresses at the drop surface which may lead to deformation and possible burst of the drop. Until the seminal work of Taylor (1966), the common perception was that the fluids are either perfect dielectric (insulator) or infinitely conducting. In either case, the "electrostatic" theory predicts that if a perfect dielectric or infinitely conducting drop is suspended in another perfect dielectric liquid, the "net" electric stresses at the interface will be normal to the interface and will point from the fluid of higher (permittivity/conductivity) to the one with lower electric permittivity, and the distribution of these stresses will be such that the drop shape at the equilibrium will always be prolate (i.e., an ellipsoid with its major axis parallel to the direction of the electric field). Since the electrostatic theory precludes an imbalance in tangential electric stresses, no fluid flow will exist at steady state. The experiments of Allan and Mason (1962) for a wide range of fluid systems, however, showed that conducting drops deformed into prolate spheroids, in agreement with the electrostatic theory, while some perfect dielectric drops deformed to oblate spheroid (i.e., an ellipsoid with its major axis perpendicular to the direction of the electric field). Motivated by anomalous observations of Allan and Mason (1962), Taylor (1966) pointed out that the fluids should not be considered perfect dielectrics or perfect conductors; rather they should be given finite permittivity and conductivity to allow for the accumulation of the free charge at the interface. The action of electric field on this charge will then lead to an imbalance in both normal and tangential stresses, and therefore, a possibility for oblate deformation. Furthermore, since the imbalance in the electrical shear stresses must be balanced by hydrodynamic shear stresses at equilibrium, the hydrodynamic shear stresses lead to fluid motion inside and outside of the drop. Since then, the Taylor's theory has been known as the "leaky-dielectric theory".

Taylor (1966) was able to justify the experimental results of Allen and Mason qualitatively using his theory by solving the "electrohydrodynamic" equations in the limit of creeping flow. However, further experiments by Torza et al. (1971) showed some discrepancies between the experimental results and the theory. To improve the theory, Ajayi (1978) extended the Taylor's linearized theory to include higher orders terms, and Baygents and Saville (1989) replaced the leaky-dielectric model by an electrokinetic model to examine the issue of electrokinetic effects raised by Torza et al. (1971). These modifications, however, did not lead to drastic improvement in the drop deformation. This led Vizika and Saville (1992) to perform new experimental investigations where they were able, through careful experimental measurements, to obtain the results that matched the theory more closely. While there is still some discrepancy, it is now generally believed that the leaky-dielectric theory is the correct "lumped-parameter" model when no net charge exists on the drop. See, for example, Feng and Scott (1996) and Vizika and Saville (1992).

* Corresponding author. Tel.: +1 618 453 7001; fax: +1 618 453 7685.
E-mail address: esmaeeli@engr.siu.edu (A. Esmaeeli).

0301-9322/$ - see front matter © 2009 Elsevier Ltd. All rights reserved.
doi:10.1016/j.ijmultiphaseflow.2009.06.008

Early interest on the subject stemmed from deformation and break up of rain drops during thunderstorm (Macky, 1931), and the effect of deformation of aerosol on optical studies of disperse systems (O'Konski and Thacher, 1953; O'Konski and Harris, 1957). The interest on the subject grew further because of its potential applications in diverse areas such as nuclear physics (Pelekasis et al., 1990), meteorology (Beard et al., 1989), chemical engineering (Basaran et al., 1989), and materials processing in microgravity (Carruthers and Testardi, 1983). More recent interest is directed toward applications involving microfluidic systems such as atomization of liquid jets by electric field in continuous inkjet printing (Mutoh, 2002), manipulation of drops in lab-on-a-chip applications by continuous electrowetting (Zeng and Korsmeyer, 2004), and design of electrorheological fluids by characterization of their rheological response (Ha and Yang, 2000), to name a few.

The literature on the stability and deformation of a drop due to exposition to an electric field is rich and the research is still ongoing. Here, we make no attempt to address all the studies, rather we refer only to a few relevant ones. The review articles by Melcher and Taylor (1969), Arp et al. (1980) and Saville (1997) present a summary of the governing electrohydrodynamics laws and their solution in the context of a planar interface separating two fluids and/or a suspended drop in quiescent and shear-driven creeping flows. Instability and deformation of a perfect dielectric/infinitely conducting drop in a perfect dielectric medium has a long history and has been extensively studied by analytical and numerical solutions (see, for example, O'Konski and Thacher, 1953, O'Konski and Harris, 1957, Miksis, 1981, Haywood et al., 1991, and Basaran et al., 1995). Computations of leaky-dielectric drops are more recent and Sherwood (1988) was perhaps the first in doing so, who simulated deformation up to break up of a drop for a wide range of permittivity and conductivity ratios using a boundary integral method. Finite Reynolds number effects have been studied by Tsukada et al. (1993, 1994) and Feng and Scott (1996) using a Galerkin finite element technique. The latter offers a comprehensive study of the deformation of a single drop at steady state as a function of the controlling parameters of the problem.

In contrast to liquid drops, the behavior of a two-dimensional filament separating two fluids in electric field is less studied. This problem finds relevance in a wide range of applications such as instability of liquid jets or bridges in electric fields, where the axis of the jet is perpendicular to the direction of the field. An analytical solution to this problem was found by Rhodes et al. (1989) in the creeping flow limit and in the context of performance degradation during separation of colloidal particles in continuous flow electrophoresis (CFE). In CFE, a thin stream of dilute colloidal particles is forced to move coaxially with a buffer fluid through a rectangular cell, where due to an applied electric field (normal to the jet axis) the fluid stream is deformed, fractioned, and the fractionated sample bands are subsequently collected at the exit of the cell. Rhodes et al. (1989), however, allowed for mass transfer through the interface by considering the normal component of fluid velocity to be continuous at the interface. Such a boundary condition is an appropriate kinematic condition for an interface separating two "immiscible" fluids during the "transient" period where the interface deforms and moves with the normal velocity that is the same as the fluid velocities at both sides, or for an interface separating two "miscible" fluids in general. While Rhodes et al. (1989) objective in using this boundary condition may have been to simply account for the interface deformation, the fact that the interface should remain stationary at steady state, implies a solution that is well-suited for a "permeable" interface.

The goal of present study is to provide a detailed understanding of the mechanism of electric field-driven fluid flow and deformation of a liquid cylinder surrounded by another liquid in a transverse electric field, in the framework of leaky-dielectric theory and in the limit of small electric field and fluid inertia. Here, the problem setup is the same as that of Rhodes et al. (1989), however, the interface is considered to be "impermeable". The results of this study are compared to those for an infinitely conducting or a perfect dielectric liquid cylinder surrounded by a perfect dielectric fluid. Also, a comparison is made between our results and those of Rhodes et al. (1989) and Taylor (1966) for a fluid drop. The results of this study may be of practical applications for EHD-driven instability of liquid jets and continuous flow electrophoresis.

2. Problem setup and nondimensional parameters

Consider a liquid cylinder of radius a surrounded by another liquid of infinite extent and exposed to a uniform electric field $\mathbf{E}_\infty$ as shown in Fig. 1. This geometrical setup can be thought of as a liquid jet moving coaxially with another liquid in the direction normal to the plane of the paper. It also resembles a "two-dimensional" liquid drop suspended in another liquid. The physical properties of the fluids are the densities, ρ_i, ρ_o, the viscosities, μ_i, μ_o, the electric permittivities, ϵ_i, ϵ_o, and the electric conductivities, σ_i, σ_o. The surface tension coefficient at the interface of the two fluids is γ. Here, the subscripts i and o are used to identify quantities inside and outside of the cylinder. This problem does not have a natural velocity or time scale. However, a velocity scale can be constructed based on the fact that the fluid flow results in from a balance of electrical and hydrodynamic shear stresses at the interface. The electric shear stress $\tau^e_{r\theta}$ scales as $q_s E_\infty$, q_s being the electric free charge per unit area, which scales as ϵE_∞. This results in $\tau^e_{r\theta} \sim \epsilon E^2_\infty$. The hydrodynamic shear stress $\tau^h_{r\theta}$ scales as $\mu u_s/a$, where u_s is the velocity scale. Considering $\epsilon E^2_\infty \sim \mu u_s/a$ leads to the velocity scale $u_s = \epsilon E^2_\infty a/\mu$. Using the physical properties of the ambient fluid and nondimensionalization leads to the flow Reynolds number $Re_f = \rho_o a u_s/\mu_o$, the electric capillary number $Ca_{el} = \mu_o u_s/\gamma$, and the electric Reynolds number $Re_{el} = u_s \epsilon_o/\sigma_o a$ as the primary nondimensional numbers of this problem, where $u_s = \epsilon_o E^2_\infty a/\mu_o$. The ratios of material properties, $R = \sigma_i/\sigma_o, S = \epsilon_i/\epsilon_o, \lambda = \rho_i/\rho_o$, $\eta = \mu_i/\mu_o$, provide a secondary set of nondimensional numbers. Here, Re_f represents the ratio of inertia force to the viscous force, Re_{el} represents the ratio of time scale of charge relaxation from the fluid bulk to the surface, (ϵ/σ), to the time scale of charge convection by the flow, (a/u_s), and Ca_{el} represents the ratio of the viscous force over the surface tension.

The key assumption in the leaky-dielectric theory is that the time scale of charge relaxation time is much less than the time scale of charge convection, so that the bulk of fluids to be free of charge. This translates to $Re_{el} \ll 1$. Assuming further that the flow is steady state, the inertial forces are small, $Re_f \ll 1$, and the

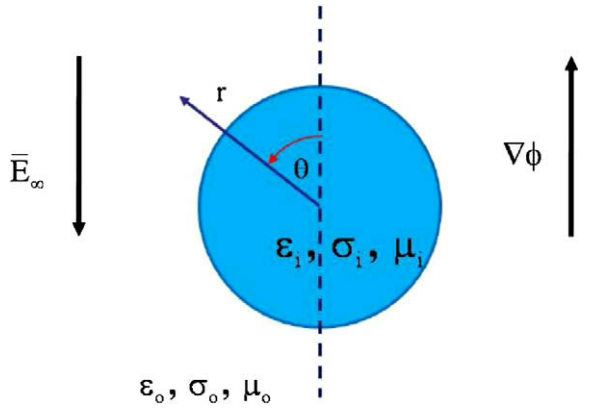

Fig. 1. The geometric setup depicting the cross section of a fluid cylinder surrounded by a pool of another fluid of infinite extension.

interface does not deform, $Ca_{el} \ll 1$, it is possible to solve the electrohydrodynamic equations analytically. To do so, we use cylindrical coordinates as shown in Fig. 1, where θ is the polar angle measured from the field direction in the counterclockwise direction and r is the radial distance from the origin.

3. Governing equations

Electrohydrodynamic deals with interaction of electric field and fluid flow. As such, the laws concerning the fluid flow and electric field and their interplay should be considered. The governing equations for steady state, incompressible, and creeping flows are the conservations of mass

$$\nabla \cdot \mathbf{u} = 0, \tag{1}$$

and momentum

$$-\nabla p + \mu \nabla^2 \mathbf{u} + \mathbf{F}^e = 0, \tag{2}$$

where $\mathbf{u}$ is the fluid velocity, p is the pressure, and $\mathbf{F}^e$ is the electric force per unit area (volume in three dimensions). ∇^2 is the Laplacian operator in polar coordinate acting on a vector.

The electric body force on a fluid has been treated by several authors, most notably by Landau and Lifhsitz (1960). Briefly, the electric force is comprised of three components and can be expressed as

$$\mathbf{F}^e = q_v \mathbf{E} - \frac{1}{2}\mathbf{E}\cdot\mathbf{E}\nabla\epsilon + \nabla\left[\rho\left(\frac{\partial\epsilon}{\partial\rho}\right)_T \mathbf{E}\cdot\mathbf{E}\right], \tag{3}$$

where the first term is the electrophoretic (Coulomb) force, the second term is the dielectrophoretic force, and the third term is the electrostriction force. The electrophoretic force is the result of action of the electric field $\mathbf{E}$ on the free charges in the fluid bulk q_v, the dielectrophoretic force stems from the nonuniformity of the electric permittivity (or the electric field), and the electrostriction force is the result of variation of the electric permittivity with the fluid density. As the above equation suggests, the electric force, in general, is discontinuous across the interface.

The first two terms in Eq. (3) vanish in the fluid bulk for leaky-dielectric fluids with constant electric properties, since $q_v = 0$ and $\nabla\epsilon = 0$, respectively. For incompressible flows, on the other hand, it is possible to group the electrostriction term with the pressure (see, for example, Smith and Melcher, 1967). Eq. (2), therefore, can be written as

$$-\nabla P + \mu\nabla^2\mathbf{u} = 0, \tag{4}$$

where

$$P = p - \rho\left(\frac{\partial\epsilon}{\partial\rho}\right)_T \mathbf{E}\cdot\mathbf{E}, \tag{5}$$

is considered a modified pressure. For nonpolar liquids, the electrostriction term can be simplified using the Clausius–Mossotti relation (Stratton, 2007):

$$\rho\left(\frac{\partial\epsilon}{\partial\rho}\right)_T = \frac{(\epsilon-\epsilon_0)(\epsilon+2\epsilon_0)}{3\epsilon_0}, \tag{6}$$

where $\epsilon_0 = 8.854\times10^{-12}$ F/m is the permittivity of the free space.

For a general dynamic systems, the basic laws of electricity and magnetism are coupled together and are represented by Maxwell's equations (Stratton, 2007). However, in the absence of an external magnetic field, and for very small dynamic electrical currents, it is possible to ignore the degree of magnetic induction and to decouple the electric and magnetic field. As was shown by Saville (1997), this is true for a fairly wide class of problems. Here, the electric field equations simplify greatly (Melcher and Taylor, 1969; Saville, 1997) and lead to

$$\nabla\times\mathbf{E} = 0, \tag{7}$$

$$\nabla\cdot(\sigma\mathbf{E}) = 0, \tag{8}$$

and

$$\nabla\cdot(\epsilon\mathbf{E}) = q_v. \tag{9}$$

Eq. (7) is the result of Faraday's law, $\partial\mathbf{B}/\partial t + \nabla\times\mathbf{E} = 0$, where $\mathbf{B}$ is the magnetic field. Since $\mathbf{B} = 0$, consequently, the electric field is irrotational. Eq. (8) is the result of conservation of electric charge, $Dq_v/Dt + \nabla\cdot\mathbf{J} = 0$, where D/Dt is the material derivative and $\mathbf{J}$ is the free electric current density. $\mathbf{J}$ is related to the electric field $\mathbf{E}$ according to the Ohm's law, $\mathbf{J} = \sigma\mathbf{E}$. Since for leaky-dielectric fluids the electric free charge migrates instantaneously to the interface, $q_v = 0$ in both fluids. Eq. (9) is the statements of Gauss's law which relates the electric displacement $\mathbf{D} = \epsilon\mathbf{E}$ to the free charge. These equations should be supplemented by proper jump conditions at the interface. Here, the electric field equations are decoupled from the momentum equation; i.e., the electric field $\mathbf{E}$ can be determined independent of the momentum equation. However, the momentum equation is coupled to the electric field equations in the fluid bulk and at the interface.

3.1. Electric field equations

Since the electric field is irrotational, it is possible to define an electric potential

$$\mathbf{E} = -\nabla\phi, \tag{10}$$

where $\nabla = (\partial/\partial r)\mathbf{e}_r + (1/r)(\partial/\partial\theta)\mathbf{e}_\theta$. For fluids with constant electric properties, Eq. (8) simplifies to $\nabla\cdot\mathbf{E} = 0$ in the fluids bulk. Substitution for $\mathbf{E}$ in terms of ϕ in this equation results in

$$\nabla^2\phi = 0, \tag{11}$$

where $\nabla^2 = (1/r)[\partial/\partial r(r\partial/\partial r)] + (1/r^2)(\partial^2/\partial\theta^2)$ is the Laplacian operator acting on a scalar in cylindrical coordinates.

3.2. Streamfunction formulation

Rather than solving the momentum and continuity equation, it is more convenient to develop an equation for streamfunction. This is done by taking curl of Eq. (4) and considering the fact that the curl of a gradient is zero and the curl of the velocity is the vorticity. This results in $\nabla^2\boldsymbol{\omega} = 0$ where $\boldsymbol{\omega}$ is the vorticity. For two-dimensional flows, $\boldsymbol{\omega}$ has only one nonzero component; i.e., $\omega_z = (1/r)[\partial(ru_\theta)/\partial r] - (1/r)(\partial u_r/\partial\theta), \omega_r = \omega_\theta = 0$. Therefore, the vorticity equation can be written as $\nabla^2\omega = 0$, where $\omega \equiv \omega_z$. In cylindrical coordinates, the components of velocity in radial and tangential direction are related to the streamfunction ψ by $u_r = -(1/r)(\partial\psi/\partial\theta)$ and $u_\theta = \partial\psi/\partial r$, where the streamfunction automatically satisfies the mass conservation equation. Substitution for u_r and u_θ in terms of ψ in the expression for ω_z results in $\nabla^2\psi = -\omega$. Taking the Laplacian of this equation leads to $\nabla^2(\nabla^2\psi) = -\nabla^2\omega$, and considering the fact that $\nabla^2\omega = 0$, leads to

$$\nabla^4\psi = 0, \tag{12}$$

where $\nabla^4 = \nabla^2(\nabla^2)$ is the biharmonic operator. Eq. (12) satisfies both the continuity and the momentum equation. Therefore, using the streamfunction formulation it was possible to reduce the number of equations, however, the penalty is to solve a higher order differential equation.

4. Solution of electric potential equation

Eq. (11) must be solved for the electric field inside and outside of the cylinder subject to proper boundary and jump conditions. It is insightful to express the jump conditions in a tangent-normal

coordinate system and to customize the resulting expressions to other coordinates afterwards. Doing so, the jump conditions are valid for a general interface in any coordinate system. In this coordinate system, $\mathbf{E} = E_t\mathbf{t} + E_n\mathbf{n}$, where $E_t = \partial\phi/\partial t$ and $E_n = \partial\phi/\partial n$, and $\mathbf{t}$ and $\mathbf{n}$ are the unit vectors tangent and normal to the interface, respectively. The following boundary conditions apply:

(i) The electric potential should remain finite inside the cylinder:

$\phi_i(0,\theta)$ should be bounded.

(ii) The electric potential across the interface should be continuous. This can be proved using a two-dimensional pillbox system spanning a portion of the interface and application of Stokes theorem on Eq. (7), $\int_A \nabla\times\mathbf{E} = \oint_C \mathbf{E}\cdot\mathbf{t}\,dS = 0$, where dS is the differential arclength along the interface. This results in $E_{t_i} = E_{t_o}$ at the interface, which implies $\phi_i = \phi_o \quad \text{at } r = a.$

(iii) The normal component of electric current density should be continuous across the interface. This can be proved by considering a two-dimensional pillbox spanning a portion of the boundary and application of Gauss theorem on Eq. (8), $\int_A \nabla\cdot(\sigma\mathbf{E}) = \oint_C \sigma\mathbf{E}\cdot\mathbf{n}\,dS$=0. This results in $\sigma_i E_{n_i} = \sigma_o E_{n_o}$ at the interface, which implies

$$\sigma_i\frac{\partial\phi_i}{\partial r} = \sigma_o\frac{\partial\phi_o}{\partial r} \quad \text{at } r = a,$$

(iv) The electric potential far away from the cylinder behaves as

$$\phi_o \sim rE_\infty\cos\theta, \quad r\to\infty.$$

This boundary condition can better be understood from Fig. 1 which suggests that the components of electric field far away from the cylinder in r and θ directions are $E_r = -E_\infty\cos\theta$ and $E_\theta = +E_\infty\sin\theta$, respectively. This translates to $\partial\phi/\partial r = E_\infty\cos\theta$ and $(1/r)\partial\phi/\partial\theta = -E_\infty\sin\theta$ as $r\to\infty$, and integrating any of these equations with respect to r or θ, respectively, leads to the above boundary condition.

Since Eq. (11) and its boundary conditions are homogeneous, separation of variables can be used to solve this equation. Taking $\phi(r,\theta) = \Lambda(r)\Theta(\theta)$, yields $d^2\Theta/d\theta^2 + k^2\Theta = 0$ and $r^2 d^2\Lambda/dr^2 + r\,d\Lambda/dr - k^2 = 0$, where k is a constant to be determined. The solution of the above ordinary differential equations are $\Lambda(r) = C_1' r^k + C_2' r^{-k}$ and $\Theta(\theta) = C_3'\cos(k\theta) + C_4'\sin(k\theta)$. Boundary condition (iv) suggests that $k = 1$ and the $\sin(k\theta)$ term must be dropped out of the expression for $\Theta(\theta)$. Therefore, the electric potential inside the cylinder can be written as $\phi_i = (C_1 r + C_2 r^{-1})\cos\theta$, where $C_1 = C_1'C_3'$ and $C_2 = C_2'C_3'$ are a new set of constants. Similarly, $\phi_o = (C_3 r + C_4 r^{-1})\cos\theta$, where C_3 and C_4 are another set of constants. To determine ϕ_i and ϕ_o, the constants must be evaluated. Boundary condition (i) results in $C_2 = 0$ and boundary condition (iv) results in $C_3 = E_\infty$. Thus, the solutions for the electric potential inside and outside the cylinder are $\phi_i = C_1 r\cos\theta$ and $\phi_o = (E_\infty r + C_4 r^{-1})\cos\theta$. To determine C_1 and C_4, boundary conditions (ii) and (iii) are imposed which results in $C_1 = 2E_\infty/(1+R)$ and $C_4 = a^2E_\infty(1-R)/(1+R)$, where $R = \sigma_i/\sigma_o$. Substitution of the expressions for C_1 and C_4 in the final expressions for ϕ_i and ϕ_o leads to the final form of the electric potential inside and outside the cylinder, respectively,

$$\phi_i = \frac{2E_\infty}{1+R}r\cos\theta \tag{13}$$

and

$$\phi_o = E_\infty\left[r - \frac{R-1}{R+1}\frac{a^2}{r}\right]\cos\theta. \tag{14}$$

4.1. The electric field

The electric field is found using Eqs. (10), (13) and (14), which yields

$$\mathbf{E}_i = -\frac{2E_\infty}{1+R}\cos\theta\mathbf{e}_r + \frac{2E_\infty}{1+R}\sin\theta\mathbf{e}_\theta, \tag{15}$$

and

$$\mathbf{E}_o = -E_\infty\left[1 + \frac{R-1}{R+1}\left(\frac{a}{r}\right)^2\right]\cos\theta\mathbf{e}_r + E_\infty\left[1 - \frac{R-1}{R+1}\left(\frac{a}{r}\right)^2\right]\sin\theta\mathbf{e}_\theta. \tag{16}$$

The corresponding expressions for Taylor's solution are given by Eqs. (A-1)–(A-4). It is insightful to rewrite Eqs. (15) and (16) in terms of the unperturbed electric field $\mathbf{E}_\infty$:

$$\mathbf{E}_i = \frac{2}{R+1}\mathbf{E}_\infty \tag{17}$$

and

$$\mathbf{E}_o = \mathbf{E}_\infty + \frac{R-1}{R+1}\left[\frac{a^2\mathbf{E}_\infty\cdot\mathbf{rr}}{r^4} - \mathbf{E}_\infty\frac{a^2}{r^2}\right], \tag{18}$$

where $\mathbf{r}$ is the position vector measured from the center. Eqs. (17) and (18) show that the electric field inside the cylinder is uniform and that the exposition of the cylinder to the electric field results in a dipole response that decays as $1/r^2$. It is interesting to note that Eqs. (13)–(18) can be readily used for perfect dielectric fluids, provided $R = \sigma_i/\sigma_o$ is replaced by $S = \epsilon_i/\epsilon_o$.

The distribution of the electric potential at the interface is fundamentally important as it determines the strength and distribution of the free charge and the electric stresses. As is seen from Eqs. (13) and (14), the ratio of the electric conductivities plays a major role in this parameter. Fig. 2 shows the contours of electric potential for conductivity ratios of $R = 0.5$, $R = 10^{-4}$, and $R = 10^4$ for the current solution (top row) as well as Taylor's (1996) solution for the corresponding axisymmetric problem (bottom row). These conductivity ratios represent, respectively, a fluid cylinder in an ambient fluid having comparable electric conductivities (silicon oil in corn oil), a perfect dielectric fluid in a perfect conductor (silicon oil in castor oil+triton), and a perfect conducting fluid cylinder in a perfect dielectric fluid (water in castor oil); see, for example, Vizika and Saville (1992) for the pertinent electric properties of these fluids. For $R = 0.5$, the contours are relatively straight equispaced horizontal lines which suggests that the electric potential varies almost linearly in the direction of the field. For $R = 10^{-4}$, the contour lines are highly concentrated in the cylinder. Since the normal component of the electric current is continuous, $J_{n_i} = \sigma_i\partial\phi_i/\partial n = J_{n_o} = \sigma_o\partial\phi_o/\partial n$, and since $J_{n_i}\sim 0$ because of low σ_i, $\partial\phi_o/\partial n$ must tend to zero at the cylinder surface to compensate for high σ_o. This is indeed the case as is seen by inspection of the slopes of the electric potential contours in the ambient fluid near the cylinder surface which are drawn normal to the surface. For $R = 10^4$, electric potential inside the cylinder vanishes and the cylinder surface becomes a line of equipotential. Here, as opposed to $R = 10^{-4}$, the tangential component of electric field, $E_t = \partial\phi/\partial t$, is zero at the interface. As such, the contour lines near the cylinder conform to its shape. Inspection of the results for Taylor's solution shows a similar trend; however, for $R = 10^{-4}$ the contours near the cylinder are less perturbed. This is because the perturbation in the electric potential dies off as $1/r^2$ in Taylor's solution (Eq. (A-2)) compared to $1/r$ for our solution.

Fig. 3 shows the vectors of the electric field along with a few selected electric field streamlines corresponding to the above cases. For all the cases, the electric field inside the cylinder is uniform as suggested by Eq. (17). For $R = 0.5$, the vectors in the ambient

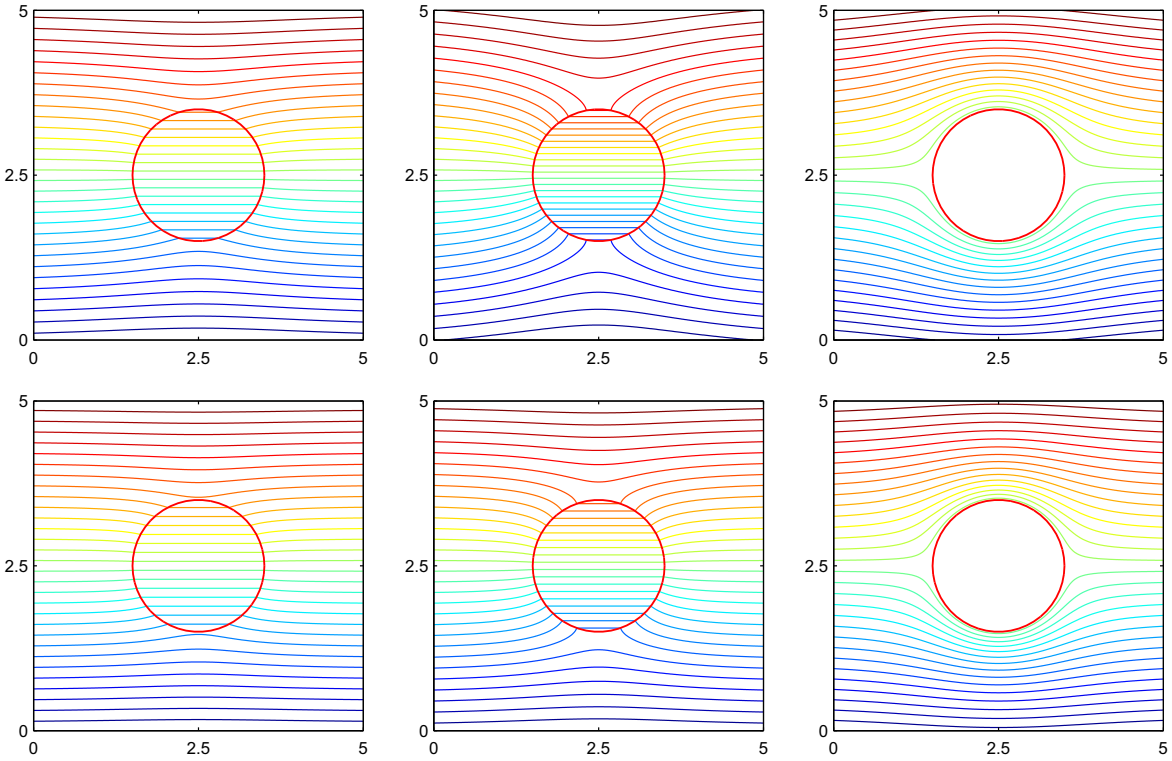

Fig. 2. Contours of electric potential for fluid systems with different electric conductivity ratios. The top row shows the contours for $R = 0.5$, $R = 10^{-4}$, and $R = 10^{4}$, respectively, for our solution. The bottom row shows the contours for the corresponding axisymmetric problem.

fluid are relatively straight vertical lines everywhere; for $R = 10^{-4}$, the electric field is stronger inside and the outer streamlines conform to the interface. For $R = 10^{4}$, the electric field vanishes inside, the vectors near the cylinder are normal to the surface, and the streamlines converge toward the cylinder as they reach equator and diverge afterward.

4.2. The electric free charge at the interface

Fluids can be classified in terms of electric conductivity σ and the dielectric constant $\epsilon_r = \epsilon/\epsilon_0$ as either conductor ($\sigma \gg 1$, $\epsilon_r = 1$), or dielectric (insulator) ($\sigma \ll 1, \epsilon_r \geqslant 1$), $\epsilon_0 = 8.854\times10^{-12}$ F/m being the permittivity of the free space. When a fluid is exposed to an external electric field, it is polarized. In the case of perfect conductors, the polarization leads to formation of free charges in the bulk of the fluids and since the electric field in a perfect conductor should be zero according to Ohm's law, the free charges will immediately migrate to the fluid boundary. The perfect dielectrics, on the other hand, do not have free electrons in their outermost atomic shells. For these fluids, the polarization leads to dipole moments which align themselves in the direction of the electric field. The surface charge per unit length q_s (area in three dimensions) can be calculated by integration of Eq. (9) over a two-dimensional pillbox spanning a portion of the boundary and application of Gauss's theorem; i.e., $\int_A \nabla\cdot(\epsilon\mathbf{E})dA = \int_A q_v\, dA$. This results in $q_s = \epsilon_o E_{n_o} - \epsilon_i E_{n_i}$, where $q_s = \lim_{A\to 0}\int_A q_v\, dA$ and $\mathbf{n}$ is the outward unit vector normal to the interface. Considering that $\sigma_i E_{n_i} = \sigma_o E_{n_o}$ at the interface, results in $q_s = \epsilon_o E_{n_o} - \epsilon_i(\sigma_o/\sigma_i)E_{n_o}$, or

$$q_s = \epsilon_o E_{n_o}\left(1 - \frac{S}{R}\right). \tag{19}$$

For the problem in hand, $E_{n_o} \equiv E_{r_o}$ and evaluation of E_{r_o} at the interface from Eq. (16) and substitution of the resulting expression into this equation yields

$$q_s = \frac{2E_\infty \epsilon_o (S-R)}{R+1}\cos\theta. \tag{20}$$

Eq. (20) suggests that the distribution of the free charge on the interface depends on the strength and direction of the electric field and the relative magnitude of R and S. Furthermore, the total free charge is zero as is evident from Eq. (20); i.e., $\oint q_s a\, d\theta = 0$. Fig. 4 shows a schematic distribution of the free charge on the interface for two cases, $R < S$ (the left frame) and $R > S$ (the right frame), along with the directions of the net electrical stresses acting on the interface (discussed in Section 4.3). For $R < S$, the upper half of the cylinder is induced with positive charges, the same in sign to the electrode that it faces, while the lower half is covered by negative charges. The opposite is true for $R > S$. If the direction of the electric field is reversed, the distribution of the charges will also be reversed. $R = S$ represents a perfect dielectric fluid in a perfect dielectric fluid and, therefore, $q_s = 0$. As will be shown shortly, the strength and distribution of the free charges have profound effect on the sense of deformation of the interface and fluid circulations in the cylinder and in the ambient fluid.

4.3. Electrohydrodynamic stresses

To derive the momentum jump condition needed in solving the momentum equation, it is necessary to find the stresses associated with the electric force. This is done by treating the electric force as divergence of the electric stress tensor; $\mathbf{F}^e = \nabla\cdot\boldsymbol{\tau}^e$. Application of Eqs. (3), (7) and (9) on this relations yields:

$$\boldsymbol{\tau}^e = \epsilon\mathbf{E}\mathbf{E} - \frac{1}{2}\mathbf{E}\cdot\mathbf{E}\epsilon\mathbf{I} + \frac{1}{2}\rho\left(\frac{\partial\epsilon}{\partial\rho}\right)_T \mathbf{E}\cdot\mathbf{E}\mathbf{I}. \tag{21}$$

Here, $\boldsymbol{\tau}^e$ is the so-called Maxwell stress tensor and $\mathbf{I}$ is the identity tensor. In this study, we use Eq. (4), where we group the electrostriction term with the pressure term in the momentum equation.

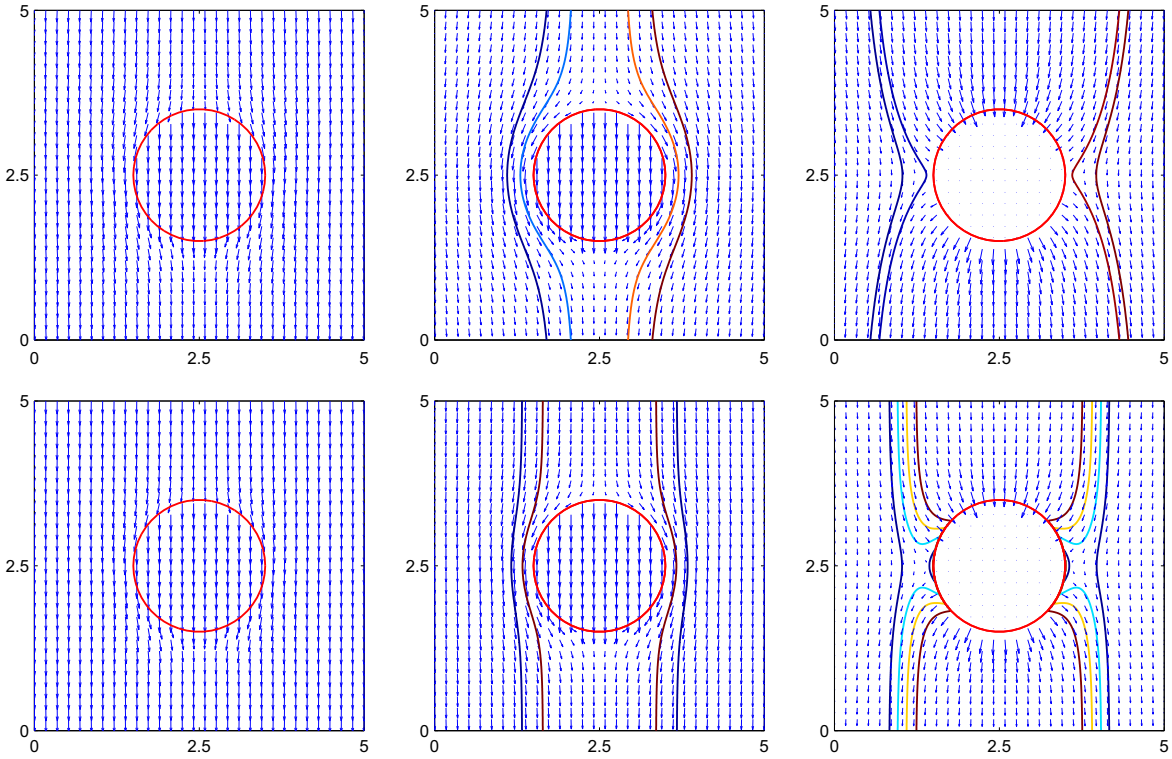

Fig. 3. Vectors of electric field for fluid systems with different electric conductivity ratios. The top row shows the vectors for $R = 0.5$, $R = 10^{-4}$, and $R = 10^{4}$, respectively, for our solution. The bottom row shows the vectors for the corresponding axisymmetric problem. The solid lines represent electric streamlines at selected levels.

As such, the Maxwell stress tensor in our formulation is simply $\boldsymbol{\tau}^e = \epsilon \mathbf{EE} - \frac{1}{2}\epsilon \mathbf{E}\cdot\mathbf{EI}$.

The electric stresses in the radial and tangential direction can be easily formulated using indicial notation; i.e., $\tau^e_{ij} = \epsilon E_i E_j - (1/2) E_k E_k \epsilon \delta_{ij}$, where i and j represents the tangent and normal directions and δ_{ij} is the Kronecker delta. This results in $\tau^e_{nn} = (\epsilon/2)\left(E_n^2 - E_t^2\right)$ and $\tau^e_{nt} = \epsilon E_t E_n$, where we have used $E^2 = E_t^2 + E_n^2$ to simplify τ^e_{nn}. For the problem in hand where $n \equiv r$ and $t \equiv \theta$, $\tau^e_{rr} = (\epsilon/2)\left(E_r^2 - E_\theta^2\right)$ and $\tau^e_{r\theta} = \epsilon E_r E_\theta$. Substitution for E_r and E_θ from Eqs. (15) and (16) in the expressions for τ^e_{rr} and $\tau^e_{r\theta}$ results in

$$\tau^e_{rr_o} = \frac{1}{2}\epsilon_o E_\infty^2 \left\{ -\left[1 + \left(\frac{R-1}{R+1}\right)^2 \left(\frac{a}{r}\right)^4 - 2\left(\frac{R-1}{R+1}\right)\left(\frac{a}{r}\right)^2\right] + 2\left[1 + \left(\frac{R-1}{R+1}\right)^2 \left(\frac{a}{r}\right)^4\right]\cos^2\theta \right\}, \tag{22}$$

$$\tau^e_{r\theta_o} = \frac{1}{2}\epsilon_o E_\infty^2 \left[\left(\frac{R-1}{R+1}\right)^2 \left(\frac{a}{r}\right)^4 - 1\right] \sin 2\theta, \tag{23}$$

$$\tau^e_{rr_i} = \frac{2\epsilon_i E_\infty^2}{(R+1)^2}(2\cos^2\theta - 1), \tag{24}$$

and

$$\tau^e_{r\theta_i} = -\frac{2\epsilon_i E_\infty^2}{(R+1)^2}\sin 2\theta. \tag{25}$$

Eqs. (22)–(25) suggest that the electric stresses are independent of the electric field polarity. The inner stresses are independent of the radial coordinate, and the perturbation in the radial and tangential electric stresses in the ambient fluid, as a result of introduction of the cylinder, die off as $1/r^2$ and $1/r^4$, respectively. The maximum shear and normal stresses (in an absolute sense) at the interface

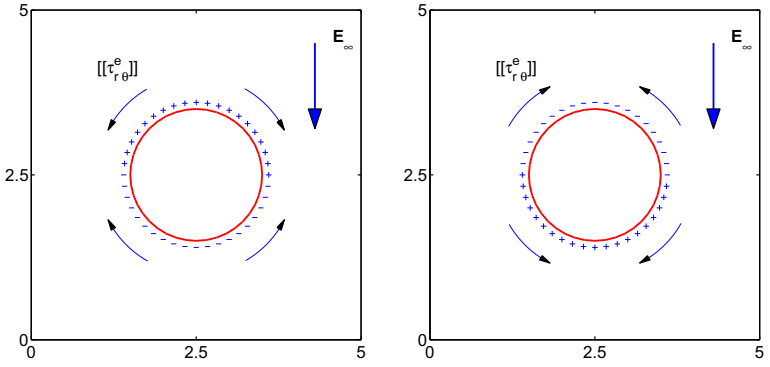

Fig. 4. A schematic figure depicting the effect of the electric field polarity and the relative magnitude of $R = \sigma_i/\sigma_o$ and $S = \epsilon_i/\epsilon_o$ on the distribution of the free electric charges at the interface. For both cases, $E_\infty < 0$. For the left frame, $R < S$, positive charges are induced at the upper half of the cylinder (drop) which faces the positive electrode and negative charges are induced at the lower half which faces the negative electrode. For this case, the electric shear stress tends to drive the flow from the poles to the equator. For the right frame, $R > S$, and the charge distribution and direction of electric shear stress are reversed.

are at $(\theta = \pm\pi/4, \pm 3\pi/4)$ and $(\theta = 0, \pi, \pm\pi/2)$, respectively. As will be shown, the tangential fluid velocity will be maximum where the shear stress is maximum and the drop deformation tends to be maximum where the normal stress is maximum.

The key parameters that affect the sense of deformation and fluid circulation are the net normal and tangential electric traction forces at the interface; i.e. $[[f^e_{sn}]] = f^e_{sn_o} - f^e_{sn_i}$ and $[[f^e_{st}]] = f^e_{st_o} - f^e_{st_i}$, where f_{sn} and f_{st} are the normal and tangential components of the electric force at the interface, respectively. The traction forces $\mathbf{f}^e_s$ at a general surface are related to the surface stresses $\boldsymbol{\tau}^e_s$ through $\mathbf{f}^e_s = \boldsymbol{\tau}^e_s \cdot \mathbf{n}$, where $\mathbf{n}$ is the unit normal vector at the interface. In a t–n coordinate system, however, $f^e_{sn} = \tau_{nn}$ and $f^e_{st} = \tau_{nt}$. Therefore, $[[f^e_{sn}]] = [[\tau^e_{nn}]]$ and $[[f^e_{st}]] = [[\tau^e_{tt}]]$. The right hand side of the above expressions are easily found to be $[[\tau^e_{nn}]] = (1/2)\epsilon_o\left(E^2_{n_o} - E^2_{t_o}\right) - (1/2)\epsilon_i\left(E^2_{n_i} - E^2_{t_i}\right)$ and $[[\tau^e_{nt}]] = \epsilon_o E_{n_o} E_{t_o} - \epsilon_i E_{n_i} E_{t_i}$, and considering the fact that $E_{t_i} = E_{t_o} \equiv E_t$ and $\sigma_o E_{n_o} = \sigma_i E_{n_i}$, results in

$$[[f^e_{sn}]] = [[\tau^e_{nn}]] = \frac{\epsilon_o}{2}\left[\left(1 - \frac{S}{R^2}\right)E^2_{n_o} + (S-1)E^2_t\right] \tag{26}$$

and

$$[[f^e_{st}]] = [[\tau^e_{nt}]] = \epsilon_o E_{n_o} E_t\left(1 - \frac{S}{R}\right) = q_s E_t. \tag{27}$$

A few interesting observations can be made from the above equations. For perfect dielectric fluids where $R = S$, Eq. (26) suggests that the sign of $[[f^e_{sn}]]$ depends on the value of S. For $S > 1$, $[[f^e_{sn}]] > 0$ and the opposite is true for $[[f^e_{sn}]] < 0$. This implies that in both cases the net normal stresses are directed from the fluid of higher electric permittivity toward the one with lower permittivity, in agreement with the experiments (see, for example, Vizika and Saville, 1992). On the other hand, for a perfect conductor in a perfect dielectric where $R \to \infty, E_t = 0$, and therefore, $[[f^e_{sn}]] = \epsilon_o E^2_{n_o}/2 > 0$, which suggests that the force is from the fluid of higher electric conductivity toward the one with lower conductivity. As will be shown in Section 6, under the above circumstances the interface will always be prolate. For leaky-dielectric fluids, however, the sense of deformation depends on the relative magnitude of R and S. Similarly, Eq. (27) suggest that for perfect dielectric fluids where $R = S$, the jump in tangential electric stresses is zero (as there is no free charge according to Eq. (19)). For a perfect conducting fluid cylinder in a perfect dielectric liquid where $R \to \infty$, on the other hand, the electric free charge is not zero. However, the jump in the tangential stresses is still zero since $E_t = 0$. The net result is that the perfect dielectric/conductor model precludes the fluid flow as it preclude the imbalance in the tangential electrical forces at the interface. For leaky-dielectric fluids, the circulation is not zero and depends on the relative magnitude of R and S.

For the problem in hand where $E_r \equiv E_n$ and $E_\theta \equiv E_t$, evaluation of E_r and E_θ at the interface from Eqs. (15) and (16) and substitution of the resulting expressions into Eqs. (26) and (27) results in

$$[[f^e_{sn}]] = [[\tau^e_{rr}]] = \frac{2\epsilon_o E^2_\infty}{(R+1)^2}[S - 1 + (R^2 + 1 - 2S)\cos^2\theta] \tag{28}$$

and

$$[[f^e_{st}]] = [[\tau^e_{r\theta}]] = \frac{2\epsilon_o E^2_\infty (S-R)}{(R+1)^2}\sin 2\theta. \tag{29}$$

The net electric stresses for the Rhodes et al. (1989) solution are the same as (28) and (29), and the corresponding expressions for Taylor's solution are given by equations (A-10) and (A-11). Fig. 5 depicts the variation of the net normal and tangential stresses at the interface for the three solutions. Here, $R = 0.252$ and $S = 0.82$, corresponding to a silicon oil drop in corn oil (Table 1). For all the solutions, the net normal stresses are compressive (i.e., $[[f^e_{sn}]] < 0$) as the expression in the bracket is negative. These stresses are maximum (in an absolute sense) at the poles, where the normal (radial) component of the electric field is maximum, and minimum at the equator, where the normal (radial) component of the electric field vanishes. See, Eqs. (15) and (16). The net shear stresses are zero at the poles and the equator, where the tangential component of the electric field vanishes and the free charge is zero, respectively. These stresses are maximum at $(\theta = \pm\pi/4, \pm 3\pi/4)$. Here, the directions of the net normal and shear stresses suggest that the electric field tends to deform the interface to an oblate shape and to drive the fluid from the poles to the equator, respectively.

5. Solution of the stream function equation

The velocity field can be found by solving the biharmonic equation (12) for the fluid inside and outside of the cylinder. To solve this equation, the following eight boundary conditions are needed:

(i) The velocity field should remain finite inside the cylinder: $u_{r_i}(0,\theta)$ and $u_{\theta_i}(0,\theta)$ should be bounded.

(ii) The no-slip boundary condition at the phase boundary: $u_{\theta_o} = u_{\theta_i}$ at $r = a$.

(iii) The no-through flow boundary condition at the phase boundary: $u_{r_o}(a,\theta) = u_{r_i}(a,\theta) = 0$.

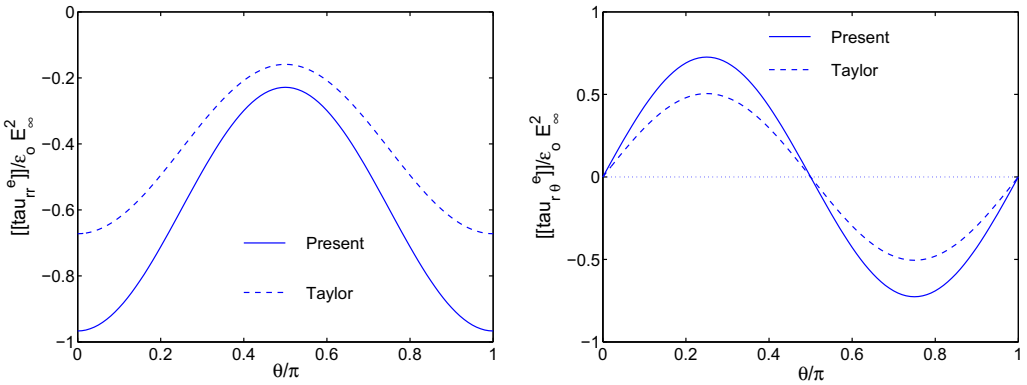

Fig. 5. Variations of net normal and shear electric stresses at the interface for $R < S$, corresponding to silicon oil in corn oil (Table 1).

Table 1
Physical properties of the fluids used. Here, $\gamma = 1.45 \times 10^{-3}$ N/m and $\epsilon_0 = 8.854 \times 10^{-12}$ F/m.

System	σ (S/m)	ϵ (F/m)	μ (kg m^{-1} s^{-1})	ρ (kg/m^3)
Silicon oil	2.67×10^{-12}	$2.66\epsilon_0$	0.0167	941
Corn oil	1.06×10^{-11}	$3.24\epsilon_0$	0.0421	914

(iv) The tangential stress balance at the phase boundary:

$$(\tau^h_{r\theta_o} - \tau^h_{r\theta_i}) + (\tau^e_{r\theta_o} - \tau^e_{r\theta_i}) = 0,$$

where $\tau^h_{r\theta} = \mu[r\partial(u_\theta/r)/\partial r + (1/r)(\partial u_r/\partial\theta)]$ is the hydrodynamic tangential shear stress.

(v) The velocity field vanishes far away from the cylinder:

$$u_{r_o} \text{ and } u_{\theta_o} \to 0 \quad \text{as } r \to \infty.$$

Notice that boundary conditions (i), (iii), and (v) each provides two boundary conditions. Since the differential equation and the boundary conditions are homogeneous, the suggested solution is of the form $\psi(r,\theta) = \Lambda(r)\Theta(\theta)$. The mathematical structure of Λ and Θ can be inferred from the behavior of the velocity field far away from the cylinder and the tangential stress balance at the interface, respectively. Far away from the cylinder, the velocity diminishes which suggests that $\Lambda(r) \sim r^n$, and since $\tau^e_{r\theta} \sim \sin 2\theta$, it is concluded that $\Theta(\theta) \sim \sin 2\theta$. Therefore, $\psi(r,\theta) = r^n \sin 2\theta$, where n is a real constant to be determined. Substitution for ψ using the above expression into Eq. (12) and simplifying yield $n(n-2)(n+2)(n-4) = 0$. The roots of this equation are $n = 0, -2, 2$, and 4. Therefore, the equations for streamfunction will be $\psi_o = (A + Br^2 + Cr^{-2} + Dr^4)\sin 2\theta$ and $\psi_i = (E + Fr^2 + Gr^{-2} + Hr^4)\sin 2\theta$, where A–H are constants to be determined. Application of boundary conditions (i) and (v) results in $E = G = 0$ and $B = D = 0$, respectively. Therefore,

$$\psi_o = (A + Cr^{-2})\sin 2\theta \tag{30}$$

and

$$\psi_i = (Fr^2 + Hr^4)\sin 2\theta. \tag{31}$$

Boundary conditions (ii), (iii), and (iv) result in, respectively

$$Ca^{-4} + F + 2Ha^2 = 0, \tag{32}$$

$$Aa^{-2} + Ca^{-4} = 0, \tag{33}$$

$$F + Ha^2 = 0, \tag{34}$$

and

$$\mu_o(12Ca^{-4} + 4Aa^{-2}) - \mu_i(4F + 12Ha^2) - \frac{2E^2_\infty \epsilon_o}{(1+R)^2}(R - S) = 0. \tag{35}$$

Solution of Eqs. (32)–(34) results in $C = -Aa^2$, $F = -A/a^2$, and $H = A/a^4$, and substitution of these coefficients in Eq. (35) results in $A = a^2\epsilon_o E^2_\infty (S-R)/[\mu_o(1+\eta)][4(1+R)^2]$. Table 2 presents the streamfunction and velocity field along with the hydrodynamic stresses for the flow inside and outside the cylinder. From the solution of u_{θ_o} given in the table, it is seen that the maximum velocity is

$$U_{max} = \frac{2A}{a} = \frac{a\epsilon_o E^2_\infty}{\mu_o(1+\eta)}\frac{(S-R)}{2(1+R)^2}, \tag{36}$$

which takes place at the interface and at angles ($\theta = \pm\pi/4, \pm 3\pi/4$). The constant coefficients in the table can be expressed in terms of U_{max} as $A = U_{max}a/2, C = -U_{max}a^3/2, F = -U_{max}/2a$, and $H = U_{max}/2a^3$. Eq. (36) suggests that the sense of fluid circulation inside and outside of the cylinder depends on the relative magnitude of R and S. Furthermore, since U_{max} is proportional to E^2_∞, the sense of fluid circulation does not depend on the electric field polarity. The streamfunctions and the velocities of the fluids, expressed in terms of U_{max}, are

$$\begin{aligned}
&\frac{\psi_o}{aU_{max}} = \frac{1}{2}\left[1 - \left(\frac{a}{r}\right)^2\right]\sin 2\theta, \quad \frac{\psi_i}{aU_{max}} = \frac{1}{2}\left[\left(\frac{r}{a}\right)^4 - \left(\frac{r}{a}\right)^2\right]\sin 2\theta \\
&\frac{u_{r_o}}{U_{max}} = \left[\left(\frac{a}{r}\right)^3 - \frac{a}{r}\right]\cos 2\theta, \quad \frac{u_{\theta_o}}{U_{max}} = \left(\frac{a}{r}\right)^3 \sin 2\theta \\
&\frac{u_{r_i}}{U_{max}} = \left[\frac{r}{a} - \left(\frac{r}{a}\right)^3\right]\cos 2\theta, \quad \frac{u_{\theta_i}}{U_{max}} = \left[2\left(\frac{r}{a}\right)^3 - \frac{r}{a}\right]\sin 2\theta
\end{aligned} \tag{37}$$

Similar expressions are presented for the axisymmetric solution in Eq. (A-13). The formulation of the Rhodes et al. solution in terms of U_{max} is involved and is not presented.

The solution just presented differs from the solution of Rhodes et al. (1989). These authors replaced boundary condition (iii) with the following boundary conditions:

(iiia) Continuity of the radial velocity at the interface

$$u_{r_o} = u_{r_i} \quad \text{at } r = a$$

and

(iiib) the balance of radial stresses at the interface

$$-(P_o - P_i) + (\tau^e_{rr_o} - \tau^e_{rr_i}) + (\tau^h_{rr_o} - \tau^h_{rr_i}) = 0,$$

where they assumed the surface tension to be negligible. Considering a solution of the form $\psi_o = (A_R a^4 r^{-2} + B_R a^2)\sin 2\theta$ and $\psi_i = (C_R r^2 + D_R a^{-2} r^4)\sin 2\theta$ and applications of boundary conditions (ii), (iii)a, (iii)b, and (iv) lead to

$$\begin{aligned}
&A_R = \frac{1}{3}F_R[R^2 + 4R + 1 - 6S], \quad B_R = F_R[4S - (R+1)^2], \\
&C_R = F_R[2S - R^2 - 1], \quad D_R = \frac{1}{3}F_R(R-1)^2, \\
&F_R = \epsilon_o E^2_\infty/[\mu_o(1+\eta)][4(1+R)^2].
\end{aligned} \tag{38}$$

Table 3 presents the streamfunction and velocity field along with hydrodynamic stresses for this solution. A summary of the solution of the axisymmetric problem by Taylor (1966) is presented in

Table 2
Solution of streamfunction, velocity, modified pressure, and hydrodynamic stresses from the present study. Notice that $j = i$ and o, for the inside and the outside fluids, respectively.

	$\frac{\psi_j}{\sin 2\theta}$	$\frac{u_{r_j}}{\cos 2\theta}$	$\frac{u_{\theta_j}}{\sin 2\theta}$	$\frac{P_j}{\mu_j \cos 2\theta}$	$\frac{\tau^h_{rr_j}}{\mu_j \cos 2\theta}$	$\frac{\tau_{r\theta_j}}{\mu_j \sin 2\theta}$	$\frac{\omega_j}{\sin 2\theta}$	Coefficient
Outside	r^{-2}	$-2r^{-3}$	$-2r^{-3}$	0	$12r^{-4}$	$12r^{-4}$	0	C
	1	$-2r^{-1}$	0	$-4r^{-2}$	$4r^{-2}$	$4r^{-2}$	$-4r^{-2}$	A
Inside	r^2	$-2r$	$2r$	0	-4	4	0	F
	r^4	$-2r^3$	$4r^3$	$-12r^2$	$-12r^2$	$12r^2$	$12r^2$	H

Table 3
Solution of streamfunction, velocity, modified pressure, and hydrodynamic stresses from Rhodes et al. (1989). Notice that $j = i$ and o, for the inside and the outside fluids, respectively.

	$\frac{\psi_j}{\sin 2\theta}$	$\frac{u_{r_j}}{\cos 2\theta}$	$\frac{u_{\theta_j}}{\sin 2\theta}$	$\frac{P_j}{\mu_j \cos 2\theta}$	$\frac{\tau^h_{rr_j}}{\mu_j \cos 2\theta}$	$\frac{\tau_{r\theta_j}}{\mu_j \sin 2\theta}$	$\frac{\omega_j}{\sin 2\theta}$	Coefficient
Outside	r^{-2}	$-2r^{-3}$	$-2r^{-3}$	0	$12r^{-4}$	$12r^{-4}$	0	$A_R a^4$
	1	$-2r^{-1}$	0	$-4r^{-2}$	$4r^{-2}$	$4r^{-2}$	$-4r^{-2}$	$B_R a^2$
Inside	r^2	$-2r$	$2r$	0	-4	4	0	C_R
	r^4	$-2r^3$	$4r^3$	$-12r^2$	$-12r^2$	$12r^2$	$12r^2$	$D_R a^{-2}$

Appendix A and Table 4 gives the pertinent information for this case. Evaluation of u_{θ_o} at $(r = a, \theta = \pi/4)$, using Table 3, results in

$$U_{max_R} = \frac{a\epsilon_o E_\infty^2}{\mu_o(1+\eta)} \frac{6S - (R^2 + 4R + 1)}{6(1+R)^2}, \tag{39}$$

as their maximum velocity. As opposed to the present and the axisymmetric solution, here the fluid flow does not vanish when the fluids are perfect dielectrics (i.e., $U_{max_R} \neq 0$ for $R = S$).

Fig. 6 shows a few equispaced streamline contours for the three solutions corresponding to a fluid system with $R = 0.252,\ S = 0.82$, and $\eta = 0.03967$. These nondimensional numbers, for example, may represent a silicon oil drop of radius $a = 25$ (mm) suspended in a corn oil (Table 1) and exposed to an electric field of strength $E_\infty = 5000$ (V/m). For this fluid system, the other nondimensional numbers are $\lambda = 1.0295,\ Re_f = 0.923,\ Re_{el} = 0.0461$, and $Ca_{el} = 0.0247$. This fluid system is the same as the one used by Tsukada et al. (1994) in their experiments. For the present and the Taylor's solution, the flow consists of four closed recirculation regions inside the cylinder that are matched with the corresponding ones in the outside. As the separation distances between the streamlines suggest, the flow is strong near the interface and gets weaker away from the surface. Here, the flow is from the poles to the equator, inline with the sign of U_{max} (Eqs. (36) and (A-12)) and $[[\tau^e_{r\theta}]]$ (Eqs. (29) and (A-11)). The streamlines, however, cross the interface in the Rhodes et al. solution. The curvatures of the streamlines seem to be higher in Taylor's and Rhodes et al. solution compared to us. Fig. 7 shows streamlines for a phase-reversed system (i.e., corn oil drop in silicon oil). For this system, the electric field is adjusted to 1000 V/m, and the resulting nondimensional numbers are $R = 3.968, S = 1.22,\ \eta = 2.5208,\ \lambda = 0.9713,\ Ca_{el} = 8.12 \times 10^{-4},\ Re_f = 0.1975$, and $Re_{el} = 0.0124$. Similar observations can be made for this system as well. The direction of flow here, however, is opposite to the previous case; i.e., it is from the equator to the poles. The sense of the circulation in the outer fluid suggests that the fluid tends to deform the drop to an oblate shape in Fig. 6 and to a prolate shape in Fig. 7. However, this is not conclusive as the interface is under normal electric stresses which may oppose the hydrodynamic stresses. Fig. 8 compares the vorticity contours corresponding to the first system. For all the solutions, the vorticity in the outer flow diminishes relatively rapidly.

Fig. 9 shows the variation of nondimensional velocities inside and outside of the cylinder versus r at $\theta = \pi/4$ for the tangential components, and at $\theta = 0$ for the radial components. These results are based on the first fluid system shown in Fig. 6, however, they give a general sense of what to expect. Several observations can be made from this figure. For all the solutions, u_{θ_o}/U_{max} is maximum at the interface and monotonically decreases away from

Table 4
Solution of streamfunction, velocity, hydrodynamic pressure, and hydrodynamic stresses from Taylor (1966). Notice that the corrections of Melcher and Taylor (1969) in the typographical error in the pressure is incorporated. Notice that $j = i$ and o, for the inside and the outside fluids, respectively.

	$\frac{\psi_j}{\sin^2\theta\cos\theta}$	$\frac{u_{r_j}}{1-3\cos^2\theta}$	$\frac{u_{\theta_j}}{\sin\theta\cos\theta}$	$\frac{P_j}{\mu(1-3\cos^2\theta)}$	$\frac{\tau^h_{rr_j}}{\mu_j(1-3\cos^2\theta)}$	$\frac{\tau_{r\theta_j}}{\mu_j\cos\theta\sin\theta}$	$\frac{\omega_j}{\sin 2\theta}$	Coefficient
Outside	r^{-2}	$-r^{-4}$	$2r^{-4}$	0	$8r^{-5}$	$-16r^{-5}$	0	$A_T a^4$
	1	$-r^{-2}$	0	$-2r^{-3}$	r^{-3}	$-6r^{-3}$	$-3r^{-3}$	$-A_T a^2$
Inside	r^3	$-r$	$-3r$	0	-2	-6	0	$+A_T a^{-1}$
	r^5	$-r^3$	$-5r^3$	$-7r^2$	$-6r^2$	$-16r^2$	$7r^2$	$-A_T a^{-3}$

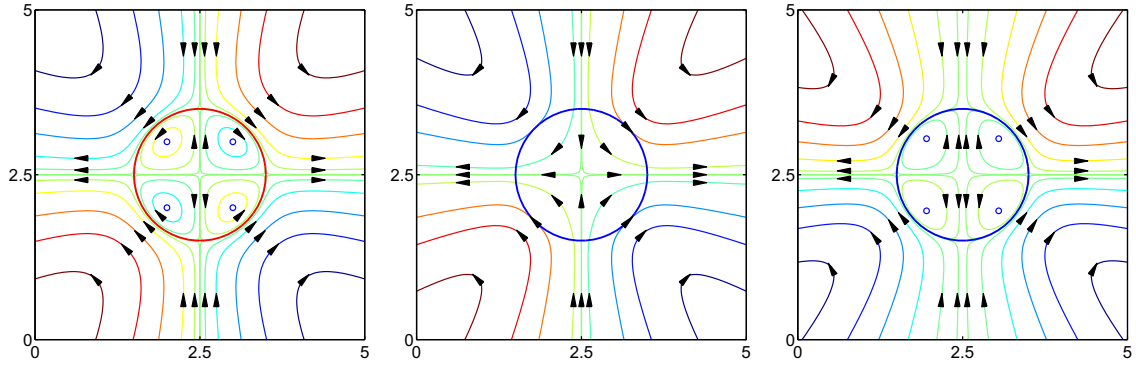

Fig. 6. Streamlines for a silicon oil (inside) in corn oil (outside). Here, $R = 0.252,\ S = 0.82,\ \eta = 0.03967,\ \lambda = 1.0295,\ Re_f = 0.923,\ Re_{el} = 0.0461$, and $Ca_{el} = 0.0247$. The frames correspond to our solution (the first frame), Rhodes et al. solution (the middle frame), and the Taylor solution (the last frame). Here, $R < S$, and as indicated in the first frame of Fig. 4, the net electric shear stresses drives the fluid from the poles to the equator.

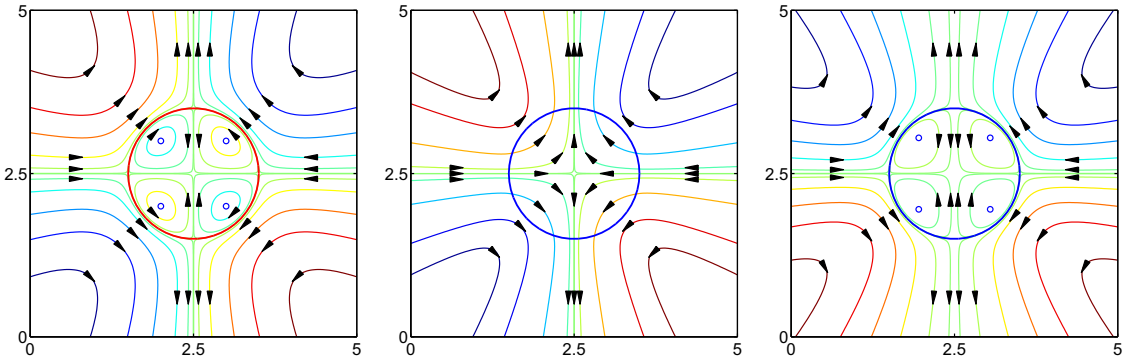

Fig. 7. Streamlines for a corn oil (inside) in silicon oil (outside). Here, $R = 3.968$, $S = 1.22$, $\eta = 2.5208$, $\lambda = 0.9713$, $Re_f = 0.1975$, $Re_{el} = 0.0124$, and $Ca_{el} = 8.12 \times 10^{-4}$. The frames correspond to our solution (the first frame), Rhodes et al. solution (the middle frame), and the Taylor solution (the last frame). Here, $R > S$, and as indicated in the second frame of Fig. 4, the net electric shear stresses drives the fluid from the equator to the poles.

the interface until it levels off to zero. u_{θ_o}/U_{max} is the same for Rhodes et al. and our solution. u_{r_o}/U_{max} is zero at the interface, goes through a maximum (in an absolute sense) at $r = \sqrt{3}a$ for our solution and $r = \sqrt{2}a$ for Taylor's solution. It gradually decays away from the interface until it levels off to zero. For Rhodes et al. solution, this velocity is maximum (in an absolute sense) at the interface and decays gradually away from the interface. u_{θ_i}/U_{max} is zero at the cylinder center, goes through a minimum at $r = a/\sqrt{6}$ for our solution and $r = a/\sqrt{5}$ for Taylor's solution, and reaches the maximum at the interface for all the solutions. u_{θ_i}/U_{max} changes sign for the current and axisymmetric solutions as the inner fluid consists of closed circulation lines. For Rodes et al. solution, the sign remains the same. The center of the inner vortices can be determined by finding the place where both u_{r_i} and u_{θ_i} are zero. This results in $r = a/\sqrt{2}$ and $\theta = \pm\pi/4, \pm 3\pi/4$ for our solution, and $r = \sqrt{3/5}a$ and $\theta = \pm 0.9553, \pm 2.5261$ for Taylor's solution, respectively. The locations of the vortices is independent of R and S. The centers of these vortices can be determined as before, however, they will also depend on R and S. For the current and Taylor solution, u_{r_i}/U_{max} is zero at the center and at the interface, it is always positive, and reaches a maximum at $r = a/\sqrt{3}$ for both solutions. On the other hand, u_{r_i}/U_{max} is not zero at the interface for the Rodes et al. solution as the mass is allowed to transfer across the boundary.

To shed more light on the nature of the recirculatory motion, we have also calculated the vorticities

$$\frac{\omega_o}{U_{max}/a} = -2\left(\frac{a}{r}\right)^2 \sin 2\theta, \quad \frac{\omega_i}{U_{max}/a} = 6\left(\frac{r}{a}\right)^2 \sin 2\theta. \tag{40}$$

The solutions for Rhodes et al. and Taylor are presented in Tables 3 and 4. These expressions suggest that the interface acts as a vortex sheet separating vorticities of opposite signs. Fig. 10 shows the variations of nondimensional vorticities for the three cases versus the nondimensional radial distance from the jet (drop) center. The vorticies (in an absolute sense) are higher for our solution and Taylor's solution compared to those of the corresponding ones for Rhodes et al. solution.

Finally, the jump in the hydrodynamic traction forces across the interface are

$$[[f^h_{sn}]] = [[\tau^h_{rr}]] = \frac{2\epsilon_o E^2_\infty (R-S)(\eta-1)}{(\eta+1)(R+1)^2}\cos 2\theta \tag{41}$$

and

$$[[f^h_{st}]] = [[\tau^h_{r\theta}]] = \frac{2\epsilon_o E^2_\infty (R-S)}{(R+1)^2}\sin 2\theta, \tag{42}$$

where $\tau^h_{rr} = 2\mu\partial(u_r)/\partial r$. Notice that Eqs. (42) and (29) are of equal value but opposite sign as is required by the tangential jump condition.

6. Interface deformation

The analysis so far was based on the premise that the interface remains circular. However, the interface is likely to deform as a result of the electric and hydrodynamic stresses. For small deformation, it is possible to calculate the distortion from circular shape using normal stress balance at the interface:

$$-(P_o - P_i) + \left(\tau^e_{rr_o} - \tau^e_{rr_i}\right) + \left(\tau^h_{rr_o} - \tau^h_{rr_i}\right) = \gamma\kappa. \tag{43}$$

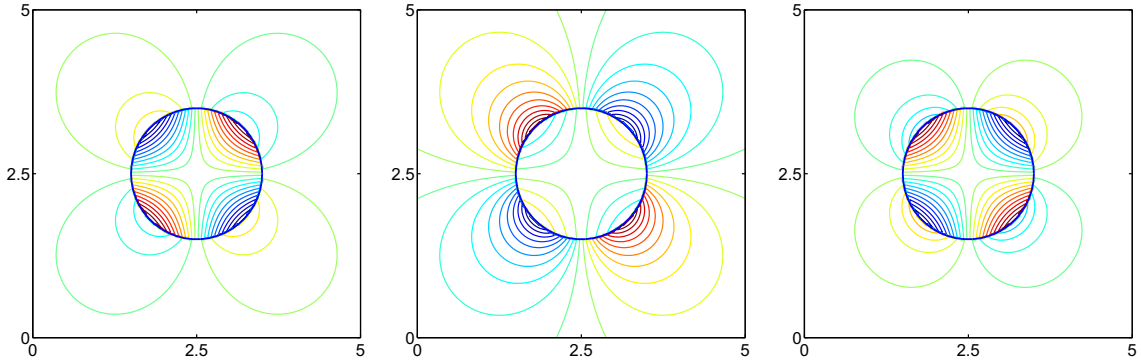

Fig. 8. Vorticity contours for the fluid system shown in Fig. 6. The frames correspond to our solution (the first frame), Rhodes et al. solution (the middle frame), and the Taylor solution (the last frame).

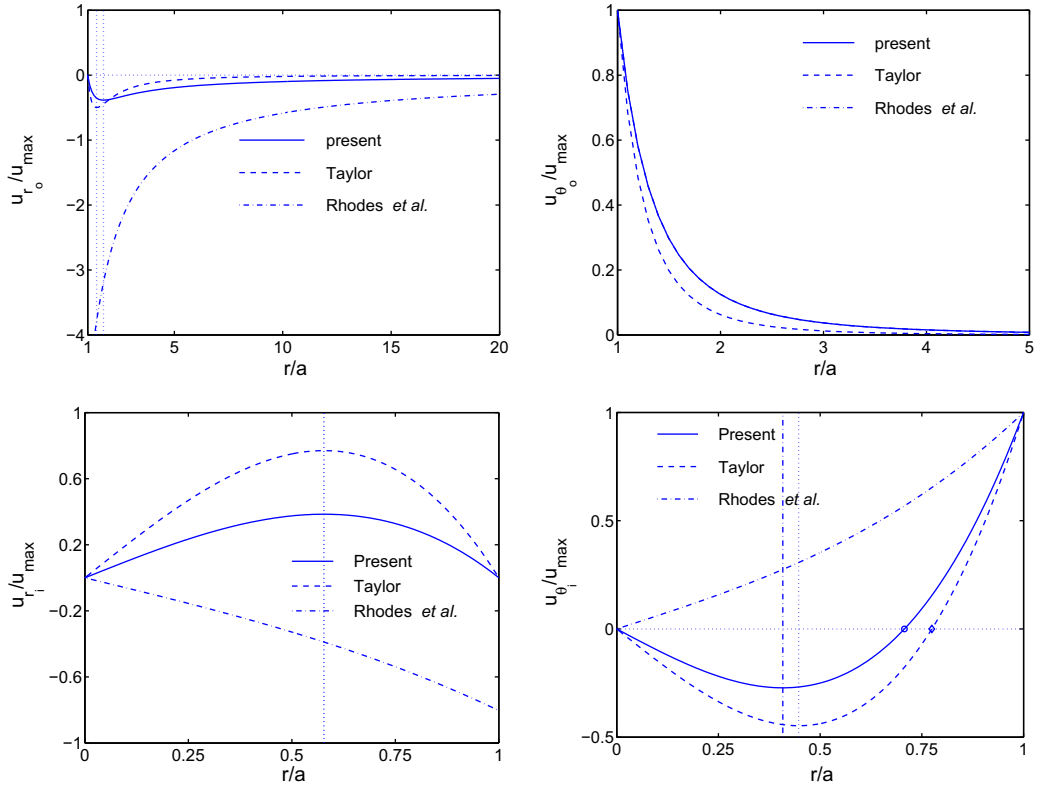

Fig. 9. Variation of dimensionless velocities with the nondimensional radial distance from the centers of the fluid cylinder (ours and Rhodes et al.) and the drop (Taylor). The top and the bottom frames correspond to the ambient and the inner flow, respectively.

In the above equation, γ is the surface tension coefficient and κ is the local curvature of the interface. To proceed, we need to calculate the pressure. This is done by writing Eq. (4) in its components form

$$\frac{\partial P}{\partial r} = \mu\left[\frac{\partial}{\partial r}\left(\frac{1}{r}\frac{\partial}{\partial r}(ru_r)\right) + \frac{1}{r^2}\frac{\partial^2 u_r}{\partial \theta^2} - \frac{2}{r^2}\frac{\partial u_\theta}{\partial \theta}\right] \tag{44}$$

and

$$\frac{1}{r}\frac{\partial P}{\partial \theta} = \mu\left[\frac{\partial}{\partial r}\left(\frac{1}{r}\frac{\partial}{\partial r}(ru_\theta)\right) + \frac{1}{r^2}\frac{\partial^2 u_\theta}{\partial \theta^2} + \frac{2}{r^2}\frac{\partial u_r}{\partial \theta}\right], \tag{45}$$

and integration of the above equations with respect to r and θ, respectively. The velocities used in the right hand side of the above equations are readily available from Table 2. This procedure yields $P_o = -4\mu_o A r^{-2}\cos 2\theta + f_o(\theta)$ and $P_o = -4\mu_o A r^{-2}\cos 2\theta + g_o(r)$, respectively, where $A = U_{max}a/2$. Equating the two expressions results in $f_o(\theta) = g_o(r) = \Pi_o$, and $P_o = -4\mu_o A r^{-2}\cos 2\theta + \Pi_o$, where Π_o is a constant. A similar procedure yields the pressure in the fluid cylinder, $P_i = -12\mu_i H r^2\cos 2\theta + \Pi_i$, where $H = U_{max}/2a^3$. Constants Π_o and Π_i can be determined by balancing the constant terms in both sides of Eq. (43). Notice that P is the modified pressure. The hydrodynamic pressure, however, can be easily found using the above expressions and Eq. 5, 6, 15 and 16. Here, we are interested in the terms that vary along the interface. The pressure jump across the interface considering θ-dependent terms is, therefore,

$$[[P]] = \frac{2U_{max}(3\mu_i - \mu_o)}{a}\cos 2\theta, \tag{46}$$

and the jump in the normal electric stresses are given by Eq. (28). Eqs. (41) and (46) are combined using $[[\sigma^h_{rr}]] = [[\tau^h_{rr}]] - [[P]]$ to find the jump in the total normal hydrodynamic traction plus the jump in the electrostriction force at the interface

$$\left[\left[f^h_{sn_{total}}\right]\right] = [[\sigma^h_{rr}]] = \frac{\epsilon_o E_\infty^2 (R-S)}{(R+1)^2}\cos 2\theta. \tag{47}$$

Eqs. (28) and (47) suggest that the cylinder radius should vary linearly with $\cos 2\theta$. Here, we consider $r = a(1 + \mathscr{D}\cos 2\theta)$, where $\mathscr{D}$ is the Taylor deformation defined as $\mathscr{D} = (y_{max} - x_{max})/(y_{max} + x_{max})$, and y_{max} and x_{max} are the end-to-end length of the cylinder cross section in the direction of electric field and the maximum breadth in the traverse direction, respectively. For a curve with a polar equation of the form $r = f(\theta)$, the curvature is $\kappa = (r^2 + 2r'^2 - rr'')/(r^2 + r'^2)^{3/2}$, where prime denotes derivation with respect to θ. This results in $\kappa = (1 + 6\mathscr{D}\cos 2\theta)/[a(1 + 2\mathscr{D}\cos 2\theta)^{3/2}]$ for our case. Simplifying the numerator and the denominator using Taylor series expansion yields $\kappa = (1/a)(1 + 3\mathscr{D}\cos 2\theta)$. Replacing $\cos 2\theta$ with $(2\cos^2\theta - 1)$ in Eq. (43) and equating the coefficients of $\cos^2\theta$ in both sides yield

$$\mathscr{D} = \frac{Ca_{el}}{3}\frac{\Phi}{(1+R)^2} \tag{48}$$

where

$$\Phi = R^2 + R + 1 - 3S, \tag{49}$$

is the characteristic function that determines the sense of interface deformation and $Ca_{el} = \mu_o u_s/\gamma$ is the capillary number defined earlier. Notice that Since Eq. (43) should be valid at any point at the interface, the constant terms on both sides of the equation are balanced and do not influence Eq. (48).

Since $Ca_{el} \sim E_\infty^2$, Eq. (48) suggests that the interface deformation scales as E_∞^2 with the electric field. This has been verified for fluid drops (see, for example, Feng and Scott, 1996). Furthermore, Eq. (48) shows how the sense of interface deformation depends on Φ; for $\Phi = 0, \mathscr{D} = 0$ and the interface remains circular, for $\Phi > 0$, $\mathscr{D} > 0$ and the interface will be prolate, and for $\Phi < 0, \mathscr{D} < 0$ and

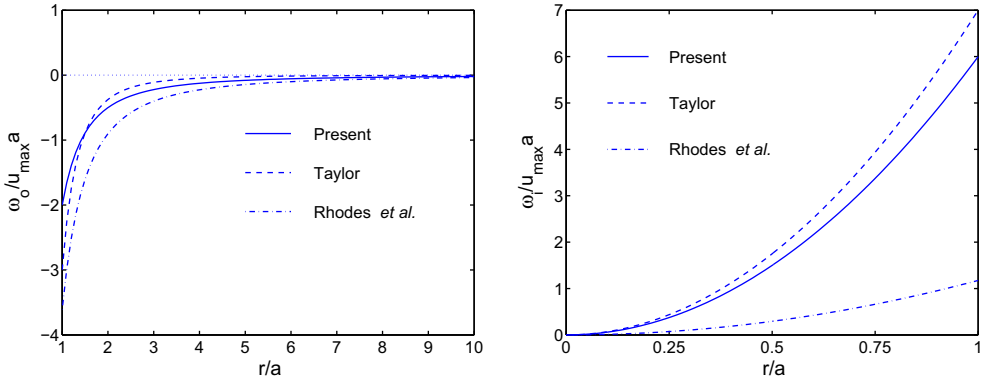

Fig. 10. Variation of dimensionless vorticities with the nondimensional radial distance from the centers of the fluid cylinder (ours and Rhodes et al.) and the drop (Taylor). The left and the right frame corresponds to the ambient and the inner flow, respectively.

the interface will be oblate. The corresponding expressions for $\mathscr{D}$ and Φ for axisymmetric solution are given by Eqs. (A-17) and (A-18). For the axisymmetric drop, the deformation is a weak function of the ratio of fluid viscosities; surprisingly however, in our solution the deformation does not depend on fluids viscosities as the jump in the total normal hydrodynamic stress is independent of the fluid viscosities. It is insightful to examine the deformation for a few limiting cases. For perfect dielectric fluids, $R = S$ and $\Phi > 0$. Therefore, the interface will always be prolate. For a perfectly conducting fluid cylinder in a perfect dielectric, $R \gg 1$, $S < 1$, and $\mathscr{D} = Ca_{el}/3 > 0$. Again, the interface will always be prolate. Fig. 11 depicts the equilibrium shape of the interface for the fluid systems shown in Figs. 6 and 7, respectively. Here, the surface tension was reduced to $\gamma = 1.45 \times 10^{-4}$ N/m to increase the interface deformation. For these systems, $\mathscr{D} = -0.0604$ and 0.0468, respectively. In terms of the aspect ratio, $\chi = y_{max}/x_{max} = (1+\mathscr{D})/(1-\mathscr{D})$, $\chi = 0.8861$ and 1.0982, respectively. The deformation may be small even for $Ca_{el} = O(1)$ since $\mathscr{D}$ depends on both Ca_{el} and Φ.

To find out the sense of interface deformation in Rhodes et al. (1989) solution, we need to examine their radial velocity at the interface. Here, a local positive radial velocity implies an interface that moves outward in the normal direction, therefore, it represent a local expansion of the interface. Similarly, a local negative radial velocity implies a local contraction of the interface. A zero radial velocity, on the other hand, corresponds to a stationary interface and, therefore, implies no interface deformation. The radial velocity at the interface is found to be $u_{r_o}(a,\theta) = -2a(A_R + B_R)\cos 2\theta$ from Table 3 and substitution for A_R and B_R from Eq. (37) yield

$$u_{r_o}(a,\theta) = u_{r_i}(a,\theta) = \frac{4}{3} a F_R \Phi_R \cos 2\theta.$$

Here, Φ_R is Rhodes et al. (1989) characteristic function which turns out to be the same as ours; i.e., $\Phi_R = \Phi$. As F_R is always positive, the sense of interface deformation will depend on Φ_R. As such, the Rhodes et al. (1989) solution predicts the same sense of interface deformation as that of our solution. The amount of deformation, however, cannot be found from their solution. To determine the interface deformation quantitatively using their solution, we modified equation (iii)b allowing for small interface deformation and accounting for the restoring force of surface tension

$$-(P_o - P_i) + \left(\tau^e_{rr_o} - \tau^e_{rr_i}\right) + \left(\tau^h_{rr_o} - \tau^h_{rr_i}\right) = \gamma\kappa.$$

The above boundary condition was used along with boundary conditions (ii), (iiia), and (iv) in the streamfunction solution, $\psi_o = (A^m_R a^4 r^{-2} + B^m_R a^2)\sin 2\theta$ and $\psi_i = (C^m_R r^2 + D^m_R a^{-2} r^4)\sin 2\theta$, to determine the unknown coefficients. Notice that as in our own solution, to use the above boundary condition we consider the interface equation as $r = a(1 + \mathscr{D}_R \cos 2\theta)$, where $\mathscr{D}_R$ is the deformation, linearize κ in terms of $\mathscr{D}_R$, write all the θ-dependent terms in terms of $\cos^2\theta$, and equate the coefficients of $\cos^2\theta$ terms in both sides of the final equation. The solution of the resulting algebraic equations yields the new constants:

$$\begin{aligned} A^m_R &= A_R - \frac{1}{3}C_0, \quad B^m_R = B_R + C_0, \\ C^m_R &= C_R + C_0, \quad D^m_R = D_R - \frac{1}{3}C_0, \\ C_0 &= \frac{3\mathscr{D}_R\gamma}{4a(\mu_i + \mu_o)}. \end{aligned} \tag{50}$$

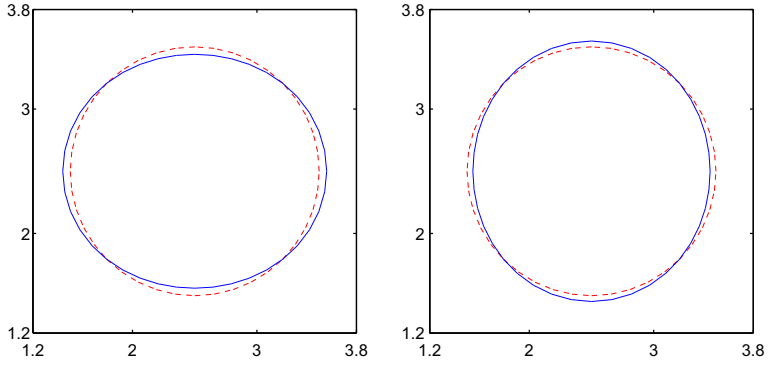

Fig. 11. Effect of relative magnitude of R and S on the interface deformation. The dashed-line represents the initial circular interface. The first frame corresponds to the system shown in Fig. 6 where $R < S$ and the second frame corresponds to system shown in Fig. 7 where $R > S$. The interface deforms to an oblate (correspondingly prolate) shape for the first (correspondingly the second) system.

The new radial velocity at the interface is found to be $u^m_{r_o}(a,\theta) = -2a(A^m_R + B^m_R)\cos 2\theta$ which can be simplified by substituting for A^m_R and B^m_R from Eq. (50)

$$u^m_{r_o}(a,\theta) = u^m_{r_i}(a,\theta) = \frac{4}{3}a(\Phi F_R - C_0)\cos 2\theta.$$

Care must be taken to interpret the above equation. In the original Rhodes et al. (1989) solution, $C_0 = 0$ and the interface will be undeformed if $\Phi = 0$. Under the current modification, however, $(4/3)aC_0\cos 2\theta$ represents the local counter displacement that is needed to bring the interface back to its circular shape. Therefore, $u^m_{r_o}(a,\theta) = 0$ serves as the equation to determine the deformation $\mathscr{D}_R$. Setting $\Phi F_R - C_0 = 0$, yields $\mathscr{D}_R = (1/3)Ca_{el}\Phi/(1+R)^2$ which is the same as Eq. (48). In other words, the degree of interface deformation using our method and Rhodes et al. (1989) method is the same.

7. Circulation–deformation map

Although the results presented here so far pertains to the behavior of a single isolated jet or a two-dimensional drop, it is possible to stipulate about the modes of interactions of two tandem/side-by-side jets/drops in dilute limit by inspection of the streamlines of the ambient fluid around a single isolated interface. The information can be used to construct a circulation–deformation map in S–R coordinates (Baygents et al., 1998). First, we note that $\Phi = 0$ represents a curve in the S–R coordinate that divides the domain into two regions of oblate and prolate deformation. Second, we examine the sense of flow circulation in the ambient fluid around the interface. For instance, consider the first frame of Fig. 6. Here, $R < S$ and the flow is from the poles to the equator. If another cylinder at a sufficiently large distance is placed in tandem beneath this cylinder, the directions of the streamlines for the second cylinder will be the same as those of the first one. This suggests that the cylinders will be attracted toward each other as the outer flow tends to move the top cylinder downward while moving the lower one upward. A similar argument for the simulation in Fig. 7, where $R > S$, suggests that the cylinders will repel each other. For side-by-side cylinders, the directions of the outer flow at the equator suggest that for $R < S$ the cylinders will repel each other while the opposite is true when $R > S$. For $R = S$, the cylinders neither repel nor attract each other due to the fluid flow as there is no flow. Therefore, line $R = S$ delineates the regions in the S–R domain where the fluid cylinders/drops attract or repel each other. When $R = S$ line and $\Phi = 0$ curve are plotted together in the S–R coordinate, the result is a map of the expected shape (oblate/prolate) and migration response (attractive/repulsive). Fig. 12 shows the deformation–circulation map and the corresponding regions, identified as region I, II, and III, respectively. In addition, the Taylor's $\Phi = 0$ curve for $\mu_i = \mu_o$ is also added to the figure. In region (I), $\Phi < 0$, $\mathscr{D} < 0$, and $R < S$. This region corresponds to oblate cylinders/drops that attract each other. In region (II), $\Phi > 0$, $\mathscr{D} > 0$, and $R < S$. This region corresponds to prolate cylinders/drops that attract each other. Finally, in region (III), $\Phi > 0$, $\mathscr{D} > 0$, and $R > S$, and the region corresponds to prolate cylinders/drops that repel each other.

8. Conclusion

The effect of a uniform electric field on the steady-state behavior of a fluid cylinder surrounded by another fluid was investigated. The governing electrohydrodynamic equations were solved for Newtonian and immiscible fluids in the framework of leaky-dielectric theory and for creeping flow regimes. The electrical and hydrodynamic stresses acting on the interface was computed and their interplay on the sense of flow circulation and interface deformation was analyzed. It was shown that the relative magnitude of the electric conductivity and permittivity ratios, $R = \sigma_i/\sigma_o$ and $S = \epsilon_i/\epsilon_o$, is the key parameter in determining the sense of fluid circulation and interface deformation. The flow field consisted of four vortical regions inside the cylinder that were matched with open circulation regions in the ambient fluid. The coordinates of the cores of the inner vortical regions depended only on the cylinder radius. It was shown that for a perfect dielectric or an infinitely conducting fluid cylinder, surrounded by another perfect dielectric fluid, the jump in electric shear stresses are always zero, but for entirely different reasons. In the former, the electric free charge at the interface is zero while in the latter, the charge exists but the tangential component of the electric field vanishes at the interface. For both cases, however, the fluid flow would cease to exist at steady state and the interface would always deform to a prolate shape. A detailed comparison was made between the fluid flow in the present study and those of Taylor (1966) and Rhodes et al. (1989) and it was shown that the results were in qualitative agreement with the Taylor's results but there were distinctly different from those of Rhodes et al. (1989) because of the difference in the interface kinematic boundary condition. The Rhodes et al. (1989) solution was modified to account for small interface deformation and restoring force of surface tension, and it was shown that the interface deformation is the same as that predicted by the current study.

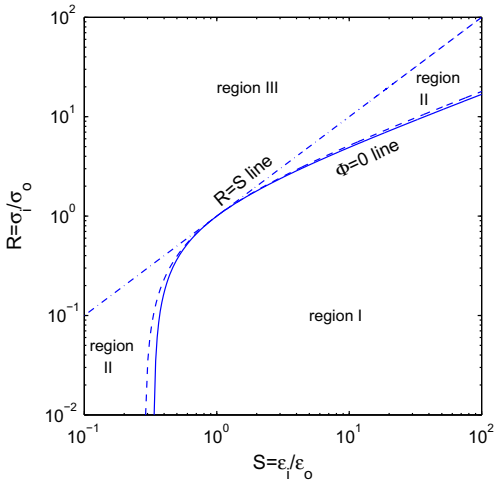

Fig. 12. Circulation–deformation map. In Region (I), the direction of the outer flow is from the poles to the equator, two tandem jets/drops deform to oblate shapes, and attract each other. In Region (II), the direction of the outer flow is from the poles to the equator, two tandem jets/drops deform to prolate shapes and attract each other. In Region (III), the direction of the outer flow is from the equator to the poles, two tandem jets/drops deform to prolate shapes and repel each other. The curve $\Phi_T = 0$ for the axisymmetric solution ($\mu_i = \mu_o$) is also added to the figure and is shown with dashed lines.

Appendix Summary of Taylor's solution

In what follows, we give a summary of Taylor (1966) analytical solution concerning the behavior of a three-dimensional drop in an electric field. Briefly, using spherical coordinates (r,θ,ϕ) and assuming axisymmetricity, $\partial/\partial\phi = 0$, the governing equation of the electric potential is $\nabla^2\phi = 0$, where $\nabla^2 = (1/r^2)[(\partial/\partial r)(r^2\partial/\partial r)] + (1/r^2\sin\theta)[(\partial/\partial\theta)(\sin\theta\partial/\partial\theta)]$. Solution of this equation subject to the pertinent boundary conditions (discussed in this study) results in the electric potential inside

$$\phi_i = \frac{3E_\infty}{2+R} r\cos\theta, \tag{A-1}$$

and outside of the drop

$$\phi_o = E_\infty\left[r - \frac{R-1}{R+2}\left(\frac{a^3}{r^2}\right)\right]\cos\theta. \tag{A-2}$$

The electric field is found using $\mathbf{E} = -\nabla\phi$, where $\nabla = (\partial/\partial r)\mathbf{e}_r + [(1/r)(\partial/\partial\theta)]\mathbf{e}_\theta$. This results in

$$\mathbf{E}_i = -\frac{3E_\infty}{2+R}\cos\theta\mathbf{e}_r + \frac{3E_\infty}{2+R}\sin\theta\mathbf{e}_\theta \tag{A-3}$$

and

$$\mathbf{E}_o = -E_\infty\left[1 + \frac{2(R-1)}{R+2}\frac{a^3}{r^3}\right]\cos\theta\mathbf{e}_r + E_\infty\left[1 - \frac{R-1}{R+2}\frac{a^3}{r^3}\right]\sin\theta\mathbf{e}_\theta, \tag{A-4}$$

Having found the electric potential and the electric field, the free charge per unit area at the interface is found, using $q_s = \epsilon_o E_{r_o} - \epsilon_i E_{r_i}$,

$$q_s = \frac{3E_\infty\epsilon_o(S-R)}{2+R}\cos\theta. \tag{A-5}$$

The electric stresses are found, using $\tau^e_{rr} = (\epsilon/2)\left(E_r^2 - E_\theta^2\right)$ and $\tau^e_{r\theta} = \epsilon E_r E_\theta$. This results in

$$\tau^e_{rr_o} = \frac{1}{2}\epsilon_o E_\infty^2\left\{-\left[1 + \frac{(R-1)^2}{(R+2)^2}\frac{a^6}{r^6} - \frac{2(R-1)}{(R+2)}\frac{a^3}{r^3}\right] + \left[2 + \frac{5(R-1)^2}{(R+2)^2}\frac{a^6}{r^6} + \frac{2(R-1)}{(R+2)}\frac{a^3}{r^3}\right]\cos^2\theta\right\}, \tag{A-6}$$

$$\tau^e_{r\theta_o} = -\frac{1}{2}\epsilon_o E_\infty^2\left[1 + \frac{(R-1)}{(R+2)}\frac{a^3}{r^3} - \frac{2(R-1)^2}{(R+2)^2}\frac{a^6}{r^6}\right]\sin 2\theta, \tag{A-7}$$

$$\tau^e_{rr_i} = \frac{9\epsilon_i E_\infty^2}{2(R+2)^2}\cos 2\theta, \tag{A-8}$$

and

$$\tau^e_{r\theta_i} = -\frac{9\epsilon_i E_\infty^2}{2(R+2)^2}\sin 2\theta. \tag{A-9}$$

The jump in the traction forces at the interface $[[\mathbf{f}^e_s]] = \mathbf{f}^e_{s_o} - \mathbf{f}^e_{s_i}$, are found using the above expressions

$$[[f^e_{sn}]] = [[\tau^e_{rr}]] = \frac{9\epsilon_o E_\infty^2}{2(R+2)^2}[S - 1 + (R^2 + 1 - 2S)\cos^2\theta], \tag{A-10}$$

$$[[f^e_{st}]] = [[\tau^e_{r\theta}]] = \frac{9\epsilon_o E_\infty^2}{2(R+2)^2}(S-R)\sin 2\theta. \tag{A-11}$$

To find the velocity field, an equation for the streamfunction is found; i.e., $E^4\psi = 0$, where $E^4 = E^2(E^2)$, and $E^2 = (\partial^2/\partial r^2) + (\sin\theta/r^2)[\partial/\partial\theta((1/\sin\theta)\partial/\partial\theta)]$. The velocities are related to the streamfunction through $u_r = (1/r^2\sin\theta)(\partial\psi/\partial\theta)$ and $u_\theta = -(1/r\sin\theta)(\partial\psi/\partial r)$. The suggested solution for the streamfunction equation is of the form $\psi = r^n\sin^2\theta\cos\theta$. Considering a solution of the form $\psi_o = (A_T a^4 r^{-2} + B_T a^2)\sin^2\theta\cos\theta$ and $\psi_i = (C_T a^{-1} r^3 + D_T a^{-3} r^5)\sin^2\theta\cos\theta$, and applications of the pertinent boundary conditions results in $A_T = -B_T = C_T = -D_T$, where

$$A_T = \frac{9a\epsilon_o E_\infty^2}{\mu_o(1+\eta)}\frac{S-R}{10(2+R)^2}. \tag{A-12}$$

From the solution of u_{θ_o} given in Table 4, it is seen that the maximum velocity is $U_{max_T} = A_T$ which takes place at the drop surface and at angles $(\theta = \pm\pi/4, \pm 3\pi/4)$. The velocities in terms of U_{max_T} can be expressed as

$$\frac{u_{r_o}}{U_{max_T}} = \left[\left(\frac{a}{r}\right)^2 - \left(\frac{a}{r}\right)^4\right](1 - 3\cos^2\theta), \quad \frac{u_{\theta_o}}{U_{max_T}} = \left(\frac{a}{r}\right)^4\sin 2\theta$$
$$\frac{u_{r_i}}{U_{max_T}} = \left[\left(\frac{r}{a}\right)^3 - \left(\frac{r}{a}\right)\right](1 - 3\cos^2\theta), \quad \frac{u_{\theta_i}}{U_{max_T}} = \frac{1}{2}\left[5\left(\frac{r}{a}\right)^3 - 3\left(\frac{r}{a}\right)\right]\sin 2\theta \tag{A-13}$$

The vorticity is found, using $\omega \equiv \omega_\phi = (1/r)[\partial/\partial r(ru_\theta)] - (1/r)(\partial u_r/\partial\theta)$,

$$\frac{\omega_o}{U_{max_T}/a} = -3\left(\frac{a}{r}\right)^3\sin 2\theta, \quad \frac{\omega_i}{U_{max_T}/a} = 7\left(\frac{r}{a}\right)^2\sin 2\theta. \tag{A-14}$$

The viscous stresses at the interface are found from $\tau^h_{r\theta} = \mu[r\partial(u_\theta/r)/\partial r + (1/r)(\partial u_r/\partial\theta)]$, $\tau^h_{rr} = 2\mu(\partial u_r/\partial r)$, and $\sigma^h_{rr} = \tau_{rr} - p$ and are given in Table 4, where we have accounted for the correction made by Melcher and Taylor (1969) to Taylor's (1966) typographical error in the pressure coefficients. The jump in hydrodynamic stresses are, therefore,

$$[[\sigma^h_{rr}]] = \frac{9\epsilon_o E_\infty^2(R-S)}{10(R+2)^2}\frac{2+3\eta}{1+\eta}(1 - 3\cos^2\theta), \tag{A-15}$$

$$[[\tau^h_{r\theta}]] = \frac{9\epsilon_o E_\infty^2(R-S)}{2(R+2)^2}\sin 2\theta. \tag{A-16}$$

Notice that Eq. (A-16) is opposite in sign but equal to Eq. (A-11) as is required by the shear stress balance.

The drop deformation is found using Eq. (43) and considering $r = a[1 + (2\mathscr{D}_T/3)(3\cos^2\theta - 1)]$ (Vizika and Saville, 1992) which results in

$$\mathscr{D}_T = \frac{9Ca_{el}}{16}\frac{\Phi_T}{(2+R)^2}, \tag{A-17}$$

where

$$\Phi_T = R^2 + 1 - 2S + \frac{3}{5}(R-S)\frac{2+3\eta}{1+\eta}, \tag{A-18}$$

is the characteristic function that determines the sense of drop deformation.

References

Ajayi, O.O., 1978. A note on Taylor's electrohydrodynamic theory. Proc. Roy. Soc. Lond. A 364, 499–507.

Allan, R.S., Mason, S.G., 1962. Particle behavior in shear and electric fields I. Deformation and burst of fluid drops. Proc. Roy. Soc. Lond. A 267, 45–61.

Arp, P.A., Foister, R.T., Mason, S.G., 1980. Some electrohydrodynamic effects in fluid dispersions. Adv. Colloid Interfaces Sci. 12, 295–356.

Basaran, O.A., Patzek, T.W., Benner, R.E., Scriven, L.E., 1995. Nonlinear oscillations and break up of conducting, inviscid drops in an externally applied electric field. Ind. Eng. Chem. Res. 34, 3454–3465.

Basaran, O.A., Scott, T.C., Byers, C.H., 1989. Drop oscillations in liquid-liquid systems. AIChE J. 35, 1263–1270.

Baygents, J.C., Rivette, N.J., Stone, H.A., 1998. Electrohydrodynamic deformation and interaction of drop pairs. J. Fluid Mech. 368, 359–375.

Baygents, J.C., Saville, D.A., 1989. The circulation produced in a drop by an electric field: a high field strength electrokinetic model. In: Wang, T.G. (Ed.), Drops and Bubbles: Third Int. Colloq. American Institute of Physics, pp. 7–17.

Beard, K.V., Ochs, H.T., Kubesh, R.J., 1989. Natural oscillations of small rain drops. Nature 342, 408–410.

Carruthers, J.R., Testardi, L.R., 1983. Materials processing in the reduced-gravity of space. Ann. Rev. Mater. Sci. 13, 247–278.

Feng, J.Q., Scott, T.C., 1996. A computational analysis of electrohydrodynamics of a leaky dielectric drop in an electric field. J. Fluid Mech. 311, 289–326.

Ha, J.-W., Yang, S.-M., 2000. Rheological responses of oil-in-oil emulsions in an electric field. J. Rheol. 44, 235–256.

Haywood, R.J., Renksizbulut, M., Raithby, G.D., 1991. Transient deformation of freely-suspended liquid drops in electrostatic fields. AIChE J. 37, 1305–1317.

Landau, L.D., Lifhsitz, E.M., 1960. Electrohydrodynamics of Continuous Media. Addison-Wesley, Reading, MA.

Macky, W.A., 1931. Some investigations on the deformation and breaking of water drops in strong electric fields. Proc. Roy. Soc. Lond. A 133, 565–587.

Melcher, J.R., Taylor, G.I., 1969. Electrohydrodynamics: a review of the role of interfacial shear stresses. Ann. Rev. Fluid Mech. 1, 111–147.

Miksis, M.J., 1981. Shape of a drop in an electric field. Phys. Fluids 24, 1967–1971.

Mutoh, M., 2002. A study on drop formation of continuous liquid jet by an electric method. Phys. Fluids 14, 1380–1388.
O'Konski, C.T., Thacher, H.C., 1953. The distortion of aerosol droplets by an electric field. J. Phys. Chem. 57, 955–958.
O'Konski, C.T., Harris, F.E., 1957. Electric free energy and the deformation of droplets in electrically conducting systems. J. Phys. Chem. 61, 1172–1174.
Pelekasis, N.A., Tsamopoulos, J.A., Manolis, G.D., 1990. Equilibrium shapes and stability of charged and conducting drops. Phys. Fluids A 2, 1328–1340.
Rhodes, P.H., Snyder, R.S., Roberts, G.O., 1989. Electrohydrodynamic distortion of sample streams in continuous flow electrophoresis. J. Colloid Int. Sci. 129, 78–90.
Saville, D.A., 1997. Electrohydrodynamics: the Taylor–Melcher leaky dielectric model. Ann. Rev. Fluid Mech. 29, 27–64.
Sherwood, J.D., 1988. Breakup of fluid droplets in electric and magnetic fields. J. Fluid Mech. 188, 133–146.
Smith, C.V., Melcher, J.R., 1967. Electrohydrodynamically induced spatially periodic cellular Stokes-flow. Phys. Fluids 10, 2315–2322.
Stratton, J.A., 2007. Electromagnetic Theory. Wiley–Interscience, New York.
Taylor, G.I., 1966. Studies in electrohydrodynamics: I. The circulation produced in a drop by an electric field. Proc. Roy. Soc. A 291, 159–167.
Torza, S., Cox, R.G., Mason, S.G., 1971. Electrohydrodynamic deformation and burst of liquid drops. Philos. Trans. R. Soc. Lond. A 269, 295–319.
Tsukada, T., Yamamoto, Y., Katayama, T., Hozawa, M., 1994. Effect of an electric field on the behavior of a drop moving in a quiescent liquid. J. Chem. Eng. Jpn. 27, 662–666.
Tsukada, T., Katayama, T., Ito, Y., Hozawa, M., 1993. Theoretical and experimental studies of circulations inside and outside a deformed drop under a uniform electric field. J. Chem. Eng. Jpn. 26, 698–703.
Vizika, O., Saville, D.A., 1992. The electrohydrodynamic deformation of drops suspended in liquids in steady and oscillatory electric fields. J. Fluid Mech. 239, 1–21.
Zeng, J., Korsmeyer, T., 2004. Principles of droplet electrohydrodynamics for lab-on-a-chip. Lab. Chip 4, 265–277.